RADC-TR-90-401
Final Technical Report
December 1990
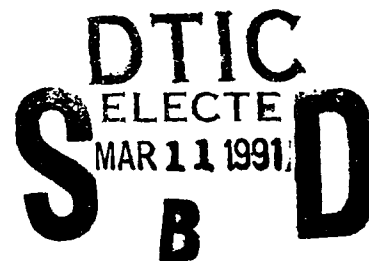
AD-A232 411

STUDIES OF NOISE IN SEMICONDUCTOR LASER ARRAYS

University of Southern California

Prof. Elsa Garmire, Ramadas Pillai,
Dr. Pedro Menendez-Valdes

DTIC
ELECTE
MAR 11 1991
S B D

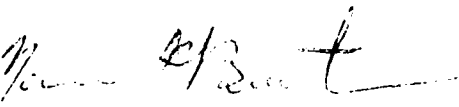*APPROVED FOR PUBLIC RELEASE; DISTRIBUTION UNLIMITED.*

Rome Air Development Center
Air Force Systems Command
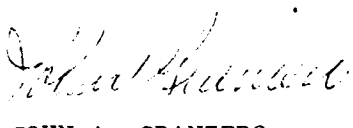Griffiss Air Force Base, NY 13441-5700

91 3 05 084

This report has been reviewed by the RADC Public Affairs Division (PA) and is releasable to the National Technical Information Service (NTIS). At NTIS it will be releasable to the general public, including foreign nations.

RADC-TR-90-401 has been reviewed and is approved for publication.

APPROVED:

NORMAN P. BERNSTEIN
Project Engineer

APPROVED:

JOHN A. GRANIERO
Technical Director
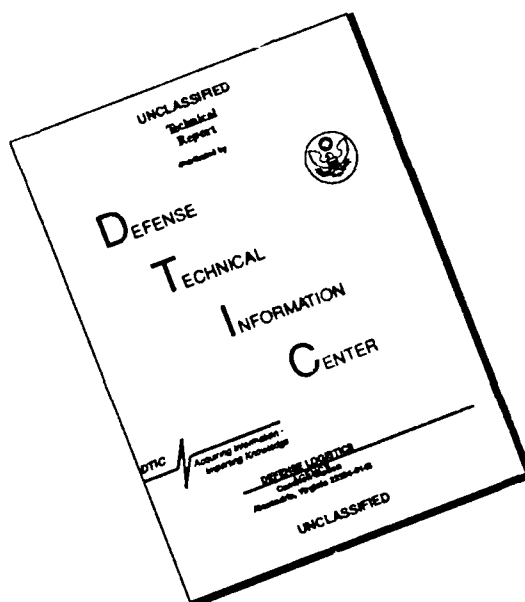Directorate of Communications

FOR THE COMMANDER:

BILLY G. OAKS
Directorate of Plans & Programs

DISCLAIMER NOTICE

THIS DOCUMENT IS BEST QUALITY AVAILABLE. THE COPY FURNISHED TO DTIC CONTAINED A SIGNIFICANT NUMBER OF PAGES WHICH DO NOT REPRODUCE LEGIBLY.

REPORT DOCUMENTATION PAGE

Form Approved
OMB No. 0704-0188

1. AGENCY USE ONLY (Leave Blank)	2. REPORT DATE	3. REPORT TYPE AND DATES COVERED
	December 1990	Final Feb 89 to Feb 90

4. TITLE AND SUBTITLE

STUDIES OF NOISE IN SEMICONDUCTOR LASER ARRAYS

5. FUNDING NUMBERS

C - F30602-88-D-0125
PE - 62702F
PR - 4519
TA - 21
WU - P8

6. AUTHOR(S)

Prof. Elsa Garmire, Ramadas Pillai, Dr. Pedro Menendez-Valdes

7. PERFORMING ORGANIZATION NAME(S) AND ADDRESS(ES)

University of Southern California
Center for Laser Studies
Los Angeles CA 90089-1112

8. PERFORMING ORGANIZATION REPORT NUMBER

93928-12/RI-62240X

9. SPONSORING/MONITORING AGENCY NAME(S) AND ADDRESS(ES)

Rome Air Development Center (DCLW)
Griffiss AFB NY 13441-5700

10. SPONSORING/MONITORING AGENCY REPORT NUMBER

RADC-TR-90-401

11. SUPPLEMENTARY NOTES RADC Project Engineer: Norman P. Bernstein/DCLW/(315) 330-4092

Report was prepared under subcontract to the University of Dayton, Graduate School of Engineering and Research, 300 College Park KL-262, Dayton OH 45469.

12a. DISTRIBUTION/AVAILABILITY STATEMENT

Approved for public release; distribution unlimited.

12b. DISTRIBUTION CODE

13. ABSTRACT (Maximum 200 words)

Measurements were made of noise in laser arrays, both commercial gain-guided and experimental 10 element index-guided. Relative Intensity Noise (RIN) was found to be comparable to single element gain-guided arrays, with approximately 15 dB more noise than from a distributed feedback (DFB) laser. Comparable results for gain-guided and index-guided lasers, with supporting theoretical studies, indicate that mode competition is probably the source of the increased noise. Because the arrays produce more power, the increased noise does not necessarily degrade the signal-to-noise ratio. The results of this study indicate that if the system is operating in the receiver-noise-limited regime (< 0.1 milliwatts of detected optical power), use of an array will increase the overall signal-to-noise ratio.

It was also shown that a reduction in laser noise can be achieved by low frequency modulation. For example, modulation at 10 MHz resulted in a decrease in noise by 5 to 10 dB at 100 MHz.

14. SUBJECT TERMS

Lasers, Optical Devices, Optical Communications, Noise Measurements

15. NUMBER OF PAGES
64

16. PRICE CODE

17. SECURITY CLASSIFICATION OF REPORT	18. SECURITY CLASSIFICATION OF THIS PAGE	19. SECURITY CLASSIFICATION OF ABSTRACT	20. LIMITATION OF ABSTRACT
UNCLASSIFIED	UNCLASSIFIED	UNCLASSIFIED	UL

ABSTRACT

Measurements were made of noise in laser arrays, both commercial
gain-guided and experimental ten-element index-guided. Relative
intensity noise was found to be comparable to single element
gain-guided arrays, with approximately 15 dB more noise than from
a distributed feedback laser. Comparable results for gain-
guided and index-guided lasers, with supporting theoretical
studies, indicate that mode competition is probably the source of
the increased noise. Because arrays produce more power, the
increased noise does not necessarily degrade the signal-to-noise
ratio. The results of this study indicate that if the system is
operating in the receiver-noise-limited regime (< 0.1 mW detected
optical power), use of an array will increase the overall signal-
to-noise ratio.

It is shown that modulation at 10 MHz causes a decrease of
between 5 and 10 dB in the noise floor at frequencies near 100
MHz. This is the first time that a reduction in noise has been
achieved by modulation at low frequency. Further reduction in
SNR may be possible with arrays if mode competition is
eliminated, by using mode-selecting elements in the cavity.

Accession For	
NTIS GRA&I	☑
DTIC TAB	☐
Unannounced	☐
Justification	
By	
Distribution/	
Availability Ccdes	
Dist	Avail and/or Special
A-1	

STUDIES OF NOISE IN SEMICONDUCTOR LASER ARRAYS

TABLE OF CONTENTS

STUDIES OF NOISE IN SEMICONDUCTOR LASER ARRAYS

I. INTRODUCTION

1. BACKGROUND

Three main characteristics have made semiconductors the most attractive sources of lasers. First, semiconductor technology is in a very high degree of development, and allows a monolithic electronic-optic interaction. Second, these lasers are suited to direct modulation by just varying the injection current. Third, electro-optic generation of light in semiconductors is very efficient and only small size and weight are required for operation. Lasers with a large emitting aperture are necessary whenever high power is required in specific applications. Laser arrays have been used for this purpose. They have better efficiency than wide single element lasers [1], and apparently allow stable transverse field distributions [2,3], even under modulation, which cannot be achieved in a broad single element due to transverse spatial hole-burning. The use of multi-element lasers instead of single broad stripe lasers does not eliminate the problem of multi- transverse mode operation and mode instability, however. Several modified structures have been proposed in order to obtain single transverse-mode operation of the array, such as distributed feedback reflectors matched to one of the specific transverse modes [4], enhancement of the side-lobes of the fundamental mode by using closer [5,6] or wider [7] stripes in the outermost elements, locking the oscillation with an external injected single wavelength [8], inducing the highest gain in the stripes of lower field confinement [9] (also called arrays of antiguides[10]), or also by combining two sets of spatially shifted arrays coupled by Y-junctions [11,12] or Talbot-imaging [13]. However, the commercially available laser arrays, at the present moment, are uncompensated arrays of gain guiding stripes, which typically can operate with multiple transverse modes. Problems such as transverse spatial hole-burning, and mode competition can be present. This, in turn, may lead to instabilities which show up as noise in the output.

2. OBJECTIVES AND METHOD OF APPROACH

It was the concern that mode competition can increase the noise in laser arrays compared to single frequency diodes which led to the study reported here. Indeed, the result of this study, both experimentally and theoretically, is that mode competition can, indeed, increase the noise, particularly at high frequencies. Experimentally it was found that single mode diodes have the smallest noise. However, for long-distance applications, where the signal has become weak, the increased power that an array offers can result in a decrease in the shot

noise of the detector, which may more than compensate for the increase in laser noise. An experimental study of arrays to determine the actual noise and output power is necessary in order to determine numerically the regime of operation where arrays are the best.

The purpose of the experimental study was to measure the relative intensity noise (RIN) of semiconductor laser arrays, both running DC and modulated. In this report the results are compared to previously published results of single laser diodes. From the RIN results, signal-to-noise ratios (SNR) are calculated. The results are that laser array noise is comparable to gain-guided laser noise, presumably because both lasers can be multi-mode. By comparison, the single-mode DFB (Distributed Feedback) lasers have approximately 15 dB smaller noise.

As with single-stripe lasers, the maximum noise occurs right at threshold and reduces strongly as the driving current increases. As with single-stripe lasers, the noise is reduced when the laser is modulated.

3. ORGANIZATION AND SUMMARY OF THE REPORT

The organization of this report is as follows:

Section II describes the principles of the laser noise measurements, including the way RIN and SNR were determined, the way the frequency response of the measurement system was taken into account, and the geometry of the laser arrays which were studied. The sub-sections are as follows:

Subsection 1 carefully defines RIN, as the mean square noise power per unit bandwidth divided by the square of the laser power.

Subsection 2 describes the experimental setup.

Subsection 3 describes how to determine RIN from the other noise components, by measuring the optical power-dependence of the noise.

Subsection 4 defines the SNR for analog modulation systems and shows how it is calculated in the presence of RIN and other noise sources. It is furthermore shown that RIN presents the ultimate limit to the SNR.

Subsection 5 describes the way in which the detector-amplifier frequency response was determined, using a white-light source.

Subsection 6 describes the geometry of the two laser arrays that were investigated, one a gain-guided array and one an index-guided array, each with ten elements.

Section III describes the results of our measurements of arrays and the comparison with measurements made on single element diodes. The first two subsections include results of noise measurements on a Spectra Diode Laboratory gain-guided laser array and on an index-anti-guided laser array, provided by TRW. The gain-guiding array had a RIN at threshold which was higher than either index-guided or gain-guided single-element lasers. At higher currents, the RIN of the array was similar to gain-guided single-element lasers. The anti-guiding array had a noise which was smaller than the gain-guided arrays below and at threshold, but a noise which at higher currents became identical to that of gain-guided arrays. This indicates that mode-competition may be important for both structures high above threshold. The last part of this section describes the reduction of RIN with modulation. It will be reported that up to 10 dB reduction in the noise floor near 100 MHz is possible with low frequency (10 MHz) modulation.

Section IV describes the results of our theoretical analysis, which indicate that the increased RIN in laser arrays over single mode DFB lasers comes from mode-competition between the two lowest order modes which choose to oscillate in a laser array.

Section V describes the conclusions of this report. This is a calculation of the SNR for arrays, comparing them to single element diodes. The result is the conclusion that there is no advantage in the SNR of using an array if the received optical power level is sufficiently high. The use of an array is an advantage if the system is receiver-noise limited. In this case an array can improve the SNR by up to 20 dB if the system is operating with low detected optical power (< 0.01 mW). Even better SNR requires single mode lasers, or reduction of noise by modulation. Ways to achieve single-mode performance with arrays seems to be an important direction for further research, as does a better understanding of the effect of modulation.

4. REFERENCES

[1]. Basov, N.G., Belenov, E.M., Letokhov, V.S., "Diffraction Synchronization of Lasers", Sov. Phys.-Tech. Phys. 10, 845-850 (1965).

[2]. Katz, J., " Phase-Locking of Semiconductor Injection Lasers", TDA Progress Rep. 42-66, 101-114 (1981).

[3]. Cninn, S.R., Spiers, R.J., "Modal Gain in Coupled-Stripe Lasers", IEEE J. Quantum Electron. QE-20, 358-363 (1984).
[4]. Syms, R.R.A., "Multiple-Waveguide Distributed Feedback Lasers", IEEE J. Quantum Electron. QE-22, 411-418 (1986).

[5]. Streifer, W., Osinski, M., Scifres, D. R., Welch, D. F., and

Cross, P.S., "Phased-array lasers with a uniform, stable supermode", Appl. Phys. Lett. **49**, 1496-1498 (1986).

[6]. Kapon, E. "The supermode structure of Phase-locked diode laser arrays with variable channel spacing", IEEE J. Quentum Electron. **QE-23**, 89-93 (1987)

[7]. Buus, J. "Semiconductor laser arrays with enhanced mode stability", IEEE J. Quantum Electron. **QE-23**, 757-759 (1987); also "Analysis of semiconductor laser arrays with high-intensity uniformity", IEEE J. Quantum Electron. **QE-24**, 22-28 (1988).

[8]. Chow, W.W., "Injection locking of an index-guided semiconductor laser array", IEEE J. Quantum Electron. **QE-22**, 655-662 (1986).

[9]. Streifer, W., Hardy, A., Burnham, R.D., Thornton, R.L., Scifres, D.R., "Criteria for design of single -lobe phased-array diode lasers", Electron. Lett. **21**, 505-506 (1985).

[10]. Botez, D., Peterson, G., "Modes of Phase-locked diode-laser arrays of closely spaced antiguides", Electron. Lett. **24**, 1042-1043 (1988)

[11]. Streifer, W., Welch, D.F., Cross, P.S., and Scifres, D. R., "Y-junction semiconductor laser arrays: Part I-Theory", IEEE J. Quantum Electron. **QE-23**, 744-751 (1987); Welch, D.F., Streifer, W., Cross, P.S., Scifres, D.R., "Y-junction semiconductor laser arrays: Part II-Experiments", IEEE J. Quantum Electron. **QE-23**, 752-756 (1987).

[12]. Hermansson, B., Yevick, D., "Analysis of Y-junction and coupled laser arrays", Appl. Opt. **28**, 66-73 (1989).

[13]. Mawst, L.J., Botez, D., Roth, T.J., Simmons, W.W., Peterson, G., Jansen, M., Wilcox, J.Z., Yang, J.J., "Phase-locked array of antiguided lasers with monolithic spatial filter", Electron. Lett. **25**, 365-366 (1989).

1.5 GLOSSARY

A = fast varying component of electric field in the crystal.
a = proportionally constant which relates to carrier density in the layer to the absolute gain per unit length.
B = band width of the spectrum analyzer.
BW = band width of the detector.
BH = buried - heterostructure.
c = the proportionality constant which relates optical power and photo curent.
c = velocity of light in vacuum.
c' = proportionality constant which relates electrical power to the square of the photo current ($= R_{eff}$)

7

$c"$ = proportionality constant which relates the electrical power across a load resistance to the detected optical power.

CO_2 = carbon dioxide

CW = continuous wave

CSP = channelled-substrate-planar

DFB = distributed feedback

d = thickness of the active layer

dBm = ten times the logarithm to the base ten of # milliwatts of power.

dB = ten times the logarithm to the base ten of the quantity.

dc = direct current

E_i = electric field of the ith mode.

f = frequency

G = combined gain of the amplifier and the detector.

G_j = local gain of the jth element.

g_i = gain of the ith mode.

GaAs = Gallium Arsenide

GaAlAs = Gallium Aluminum Arsenide.

hf = high frequency.

I_D = detector current.

I = nearfield intensity profile

I_b = bias current of the laser.

I_i = nearfield intensity profile of the ith mode.

I_{th} = threshold bias current of the laser.

i = imaginary unit.

i_{shot} = shotnoise current.

J_g = current density in the gain elements.

J_{gap} = current density in the gaps.

J_{DC} = DC current (bias current) levels through the laser.

$J_{laser\ element}$ = current density in the gain elements.

k_o = free space wave-vector.

k = wave vector in the medium.

L = length of the resonator or laser.

m = current modulation index.

MQW = multiple quantum well.

n = refractive index.

n_c = refractive index of the cover.

n_g = refractive index of the guide.

n_s = effective index of the substrate.

n_j = effective index of the jth layer.

N_j = carrier density in the j_{th} layer.

N_{tr} = transparency threshold carrier density.

N = carrier density.

N_{eff} = complex effective index of the mode.

n_{eff} = effective index.

NPS = narrow-planar stripe.

NOS = native oxide stripe

P = the total instantaneous optical power which is a sum of signal power and noise power.

P_n = the noise power.

P_o = average optical power (also signal power).

P_e = electrical signal power level after amplification.

$P_{n,shot}$ = the noise component due to shot noise.

$P_{n,b}$ = the noise component due to shot noise.

$P_{n,b}$ = background noise measured by the spectrum analyzer.

$P_{n,RIN}$ = noise component due to laser RIN.

$P_{n,tot}$ = the total noise measured by spectrum analyzer.

P_{el} = the dc power dissipated across the load resistance R_{eff} due to the detector current I_D.

P_i = photon density in the ith mode.

P_{opt} = instantaneous optical power.

PCW = plano-convex waveguide.

q = electronic charge

R = antiguiding parameter

RIN = relative intensity noise.

rf = radio frequency

r_J = ratio of the current density in the gaps to that in the gain elements.

R_{eff} = effective input resistance of the amplifier (also of the spectrum analyzer).

SNR = signal to noise ratio.

SNR_{th} = signal to noise ratio limited by thermal (background) noise.

SNR_{shot} = signal to noise ratio limited by shot noise.

SNR_{RIN} = signal to noise ratio limited by RIN of the laser.

SNR_{tot} = total signal to noise ratio.

SDL = Spectra Diode Lab.

S_e = spectral density function.

TE = transverse electric.

TM = transverse magnetic

t_{th} = time delay between the starting of simulation and the switching of bias current.

V = normalized guide width.

γ = spontaneous emission factor.

Γ_{ij} = fractional optical power of the ith mode in the jth layer.

β = propagation constant of the mode.

τ_s = spontaneous recombination carrier lifetime.

τ_p = spontaneous photon lifetime.

ϕ = the "envelope function" (slowly varying component) of the electric field in the crystal.

λ = wavelength of light in vacuum.

II. MEASUREMENT OF INTENSITY NOISE

1. DEFINITION OF RELATIVE INTENSITY NOISE

This subsection defines Relative Intensity Noise (RIN) of a laser beam. First, the term noise will be carefully defined. The term noise will be used to represent any random or chaotic (which may include non-linear physical processes not understood such as mode competition) electromagnetic fields which occupy the same (modulation) spectral region as that occupied by some "signal". It will be most useful to consider noise in the frequency domain since the measurement of noise is carried out in the frequency domain. When the optical power from a laser, modulated at frequency f, exhibits noise, the noise may defined in the frequency domain as the deviation of the physically-measured optical power P(f) from the expected optical power $P_o(f)$:

$$P_n(f) = P(f) - P_o(f), \qquad (1)$$

such that $<P_n(f)> = 0$ where $< >$ denotes the time average.

It is clear that any measurement of laser power P(f) is subject to an uncertainty due to the random nature of the noise, $P_n(f)$. While $<P_n(f)> = 0$, the mean square of the power is not zero and represents a measure of the noise. Thus, the quantity defining the noise of the laser power is $<P_n(f)^2>$.

To measure $<P_n(f)^2>$, measurements of the detected power will be made with an rf spectrum analyzer. How the spectrum analyzer works is now described. The optical power P(f) is detected using a photodiode and converted to a photo-current, $I_D(f)$. Assuming that no additional noise is generated by the process of generation of photo-current and the response of the detector is frequency independent, the detector current is proportional to the optical power:

$$I_D(f) = c\ P(f), \qquad (2)$$

where c is a constant. This electrical signal can be analyzed using an rf spectrum analyzer. The spectrum analyzer passes the electrical power through a filter, then performs a time-average. The electrical power is proportional to square of the detector current and to the square of the optical power:

$$P_e(f) = c'\ I_D(f)^2 = c''\ P(f)^2, \qquad (3)$$

10

where c' and c" are constants. Both optical modulation signals and noise can be determined by the rf spectrum analyzer, because the measured electrical power is proportional to the square of the optical power (square of the photo-current). Thus, the time-average electrical power measured by the spectrum analyzer in a narrow bandwidth B with a center frequency f defines the <u>spectral density function</u> $S_e(f)$ through

$$<P_e(f)> = S_e(f) * B. \tag{4}$$

The spectral density function is defined as the optical power squared within a given bandwidth whether or not the laser is modulated. When the laser is running CW, however, the spectral density measured will only be noise. In this case it is useful to define <u>Relative Intensity Noise</u> (RIN):

$$RIN = \frac{S_e(f)}{P_e(DC)} . \tag{5}$$

As expressed here, this is in units of electrical power from the photo-current. It may be convenient to define RIN in terms of optical power. In this case [1]

$$RIN = \frac{S_o(f)}{<P_o>^2} = \frac{<P_n^2(f)>}{<P_o>^2 \, B} , \tag{6}$$

where the "optical" spectral density $S_o(f) = S_e(f)/c"$, $<P_o>$ is the time average optical power and $<P_n^2(f)>$ is the mean square optical power measured over a band-width of B.

RIN is usually expressed in dB/Hz. RIN, being a property of the laser beam, cannot be changed by attenuating the laser beam, using, for example, a neutral density filter. It is a convenient quantity to compare the quality of two lasers (with respect to noise performance) having different output power.

2. EXPERIMENTAL SETUP

The basic setup to measure the relative intensity noise (RIN) is given in Figure II-1. The laser source whose noise characteristic is to be measured is driven by a variable, low noise current source. A portion of the light emitted is incident directly (sometimes through a neutral density filter) on the face of the detector (of band-width 350 MHz) causing photo-current directly proportional to the incident light power. The recovered RF signal is amplified (40dB) using a low noise amplifier (with 1 GHz band-width and 2 dB noise figure) then analyzed using an rf spectrum analyzer.

We have considered the various possible noise sources

11

which can contribute to the noise measured by the spectrum
analyzer. They include the noise generated by the various
electronic components used in the experiment and the quantum
shot-noise generated by the detector, as well as any laser noise.
The overall contribution from the background noise can be
measured directly from the background noise measured by the
spectrum analyzer when the laser light is shut off. However, the
noise of the power supply which drives the laser will not be
included in this background noise so we have measured it
separately. An ILX 3620 ultra-low noise current source has been
used to drive the laser. It was found that the noise decreases
with frequency and for frequencies greater than 5 Hz, the noise
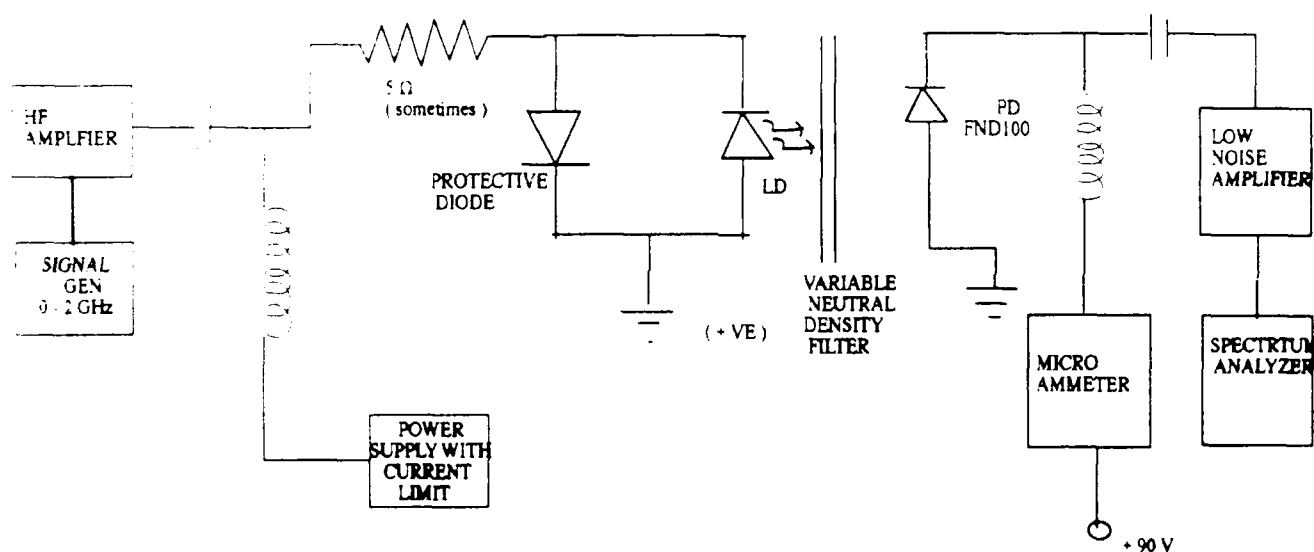is less than the noise floor of -135.7 dBV (which corresponds to

FIG. II-1. Schematic drawing of the experimental setup used for
the measurement of Relative Intensity Noise.

a root mean square noise voltage of 0.16 micro volts per $\sqrt{Hz}$), measured over a voltage drop of 1.2 V. Therefore for the RIN measurement (which is in the MHz regime), it is safe to assume that the noise of the power supply is negligibly small. Other noise sources are discussed in the following section.

3. ANALYSIS OF MEASUREMENT DATA

a. Various components of noise

The spectral density of the noise measured by the spectrum analyzer is composed of three un-correlated components:

Component 1: The incident power dependent shot noise generated by the detector. The origin of shot noise is the quantum nature of the generation of charge carriers at the detector. The quantum shot noise is essentially frequency-independent (with a white noise spectrum). The mean square noise per unit band-width in the photo-current due to the shot-noise is given by

$$<i^2_{shot}> = 2\ q\ I_D, \tag{7}$$

where q is the electronic charge and I_D is the mean photo-current in the detector. If the effective input resistance of the amplifier is given by R_{eff}, the input noise power to the amplifier would be equal to $<i^2_{shot}>\ R_{eff}$ per unit band-width. This input power is amplified by a factor of G and is measured by the spectrum analyzer over a band-width B. Thus the shot-noise power measured by the spectrum analyzer in band width B is given by

$$P_{n,shot} = 2\ q\ I_D\ B\ G\ R_{eff}. \tag{8}$$

Component 2: The incident power-independent noise of the detector electronics. This includes thermal noise of resistors, spectrum analyzer noise, amplifier noise and the shot noise due to the dark current of the detector. This noise is independent of the incident optical power level and can be measured directly from the noise floor of the spectrum analyzer (with no input light). This background noise will be represented as $P_{n,b}$.

Component 3: The noise caused by the laser RIN. This noise also depends on incident optical power. The noise power due to laser RIN in band-width B is given by $S_e(f)\ B$. This noise power after amplification by a factor of G and using equation (5), with $P_e(DC) = I_D^2 R$ becomes,

$$P_{n,RIN} = RIN\ I^2_D\ R_{eff}\ B\ G. \tag{9}$$

b. Decomposition of noise

13

Note that (7) depends linearly on I_D (and therefore on mean optical power P_O) while (9) depends quadratically on I_D and P_O. Thus, For every 1 dB increase in the incident optical power, there will be a 1 dB increase in the noise component due to the shot noise, no effect on the back-ground noise and a 2 dB increase in the electrical noise component due to the laser RIN. Therefore, a different noise mechanism dominates in different detected power level ranges as shown schematically in Figure II-2. This characteristic can be used to decompose the three noise components and to evaluate RIN from the noise measurement result. The noise measured by the spectrum analyzer is given by

$$P_{n,tot} = P_{n,shot} + P_{n,b} + P_{n,RIN}. \qquad (10)$$

Using equation (9) we have,

$$RIN = \frac{P_{n,tot} - P_{n,shot} - P_{n,b}}{P_{el} \, B \, G} , \qquad (11)$$

where $P_{el} = I^2_D \, R_{eff}$.

c. Typical numerical example

Consider the measurement of RIN at 100 MHz when the laser is biased at 200 mA and the band-width of the spectrum analyzer is 100 kHz. In the absence of laser light the spectrum analyzer showed a noise level of -86 dBm (at 100 MHz), which corresponds to an electrical power of 2.5×10^{-12} W. In the presence of laser light (about 10mW of power, only a fraction of which is collected by the detector) the noise level was -63 dBm (= 5×10^{-10} W) and the detector gave a dc current of 0.172 mA. The contribution of the shot noise at the spectrum analyzer is given by the equation (8), with R_{eff} = 50 ohms and G = 6792 (at 100 MHz). Thus the shot noise power is calculated to be equal to 1.87×10^{-12} W. The noise component due to laser RIN is obtained by subtracting the thermal noise and the shot noise from the total noise power, which is equal to 4.97×10^{-10} W. Therefore, the RIN in this case is given by

$$RIN = \frac{P_{n,RIN}}{I^2_D \, B \, R_{eff} \, G} = -123 \text{ dB/Hz} \qquad (12)$$

This high value of RIN corresponds to a bias current close to the threshold bias current of the laser and hence is not a typical value for strongly driven lasers.

4. SNR FOR ANALOG MODULATION SYSTEMS

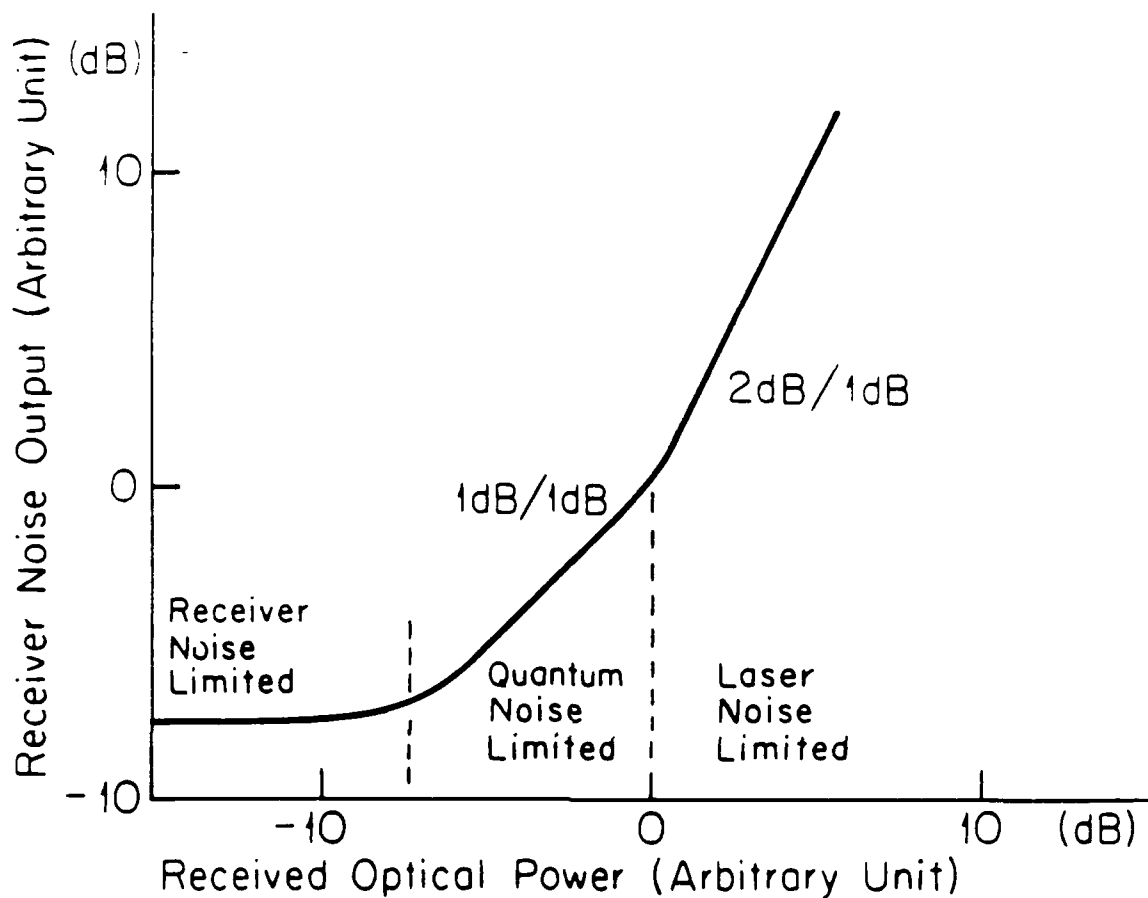From the system design point of view, RIN of the laser is

FIG.II-2. Typical receiver noise output versus received optical
power. The slope of the curve in the laser noise
limited regime and the quantum noise regime are 2dB/1dB
and 1dB/1dB respectively.

one of the most important considerations since it imposes an ultimate limit on the available signal-to-noise ratio (SNR) of the system. To show this limitation, consider the system SNR for a fiber optic sub-carrier system. Assume that the laser light is modulated by an RF signal to a modulation depth m, so that the optical power,

$$P_{opt}(f,t) = P_o (1 + m \cos 2\pi ft).\qquad(13)$$

The detected RF power will be proportional to $(m P_o)^2/2$. Using equation (3), the electrical signal power level after amplification to a factor G, is given by

$$P_e = (1/2) m^2 c" G P_o^2.\qquad(14)$$

The back-ground noise observed at the spectrum analyzer is, as before, $P_{n,b}$. The shot noise component is given (from equation (8)) by

$$P_{n,shot} = 2 q B G c" R_{eff} P_o,\qquad(15)$$

and the noise component due to laser RIN is given (from equation (9) by

$$P_{n,RIN} = B G c" RIN P_o^2.\qquad(16)$$

Assuming m = .04, c" = 5.76/W (estimated assuming a detector quantum efficiency of 50%), B = 4 MHz, G = 10000, RIN = -123 dB/Hz, $P_{n,b}$ = 2.5 x 10^{-12} W (measured), R_{eff} = 50 ohms, the following quantities are determined:

SNR due to thermal (or background electrical) noise,

$$SNR_{th} = 1.84 \times 10^{13} P_o^2. \qquad (P_o \text{ in Watts}) \qquad (17)$$

SNR due to shot noise,

$$SNR_{shot} = 2.12 \times 10^8 P_o. \qquad (P_o \text{ in Watts}) \qquad (18)$$

SNR due to laser noise,

$$SNR_{RIN} = m^2/(2 B RIN) = 26 dB .\qquad(19)$$

Now, for every 1dB increase in the detected optical power, SNR_{th} improves by 2 dB, SNR_{shot} improves by 1 dB and there is no effect on SNR_{RIN}. This means that no matter how high the received optical power, the system SNR will be limited by the laser noise. Table I gives a comparison of the SNR's with two

optical power levels at the detector, $P_0 = 0.1$ mW and 1.0 mW. This example shows how the RIN of a laser can limit the SNR of an analog modulation system. This example was chosen for a laser close to threshold, with high RIN. In the conclusion section a comparison of the performance of lasers operating at normal operating conditions will be presented.

Table I: Signal to Noise Ratio at two different power levels

Optical Power	0.1 mW	1 mW	increase of 10 dB
SNR_{th}	52 dB	72 dB	improved by 20 dB
SNR_{shot}	43 dB	53 dB	improved by 10 dB
SNR_{RIN}	26 dB	26 dB	no change
SNR_{TOT}	25.9 dB	25.99 dB	very little improvement.

5. DETERMINATION OF THE DETECTOR-AMPLIFIER GAIN G

Both the detector and the amplifier have their own contribution to the small signal modulation frequency response and it is necessary to determine this gain as a function of frequency. This is calculated from data obtained from shot noise measurements using white light as the noise-free source.

The setup for the measurement of shot noise using white light is as shown in Figure II-3. The microscope lamp is a broad band source with negligible excess noise far from 60 Hz. Hence the noise measured using this white light source is entirely due to the photo-current shot noise and the background noise $P_{n,b}$. The light from the microscope lamp is focused on the detector using a focussing lens and the resultant detector current is amplified and its spectrum is analyzed. Let $P_{n,f}$ be the measured noise power as a function of frequency. The dc current in the photo-detector is also monitored for calculating theoretical shot noise.

Since the observed noise spectrum, $P_{n,f}$, is the sum of the two uncorrelated noise components, the background $P_{n,b}$ and the amplified shot-noise $P_{n,shot}(amplif)$, we have,

$$P_{n,shot}(amplif) = P_{n,f} - P_{n,b} \qquad (20)$$

where the background noise $P_{n,b}$ is determined by shutting off the microscope lamp. The frequency response of the gain as a function of frequency is calculated by

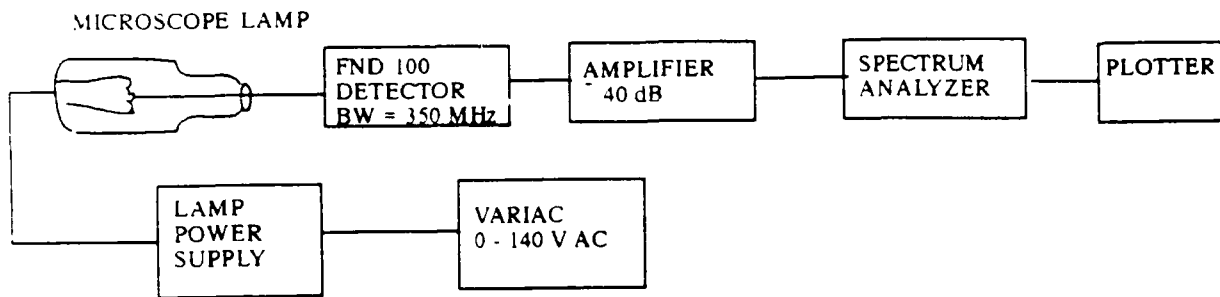$$G = \frac{P_{n,shot}(amplif)}{P_{n,shot}(calc)}, \qquad (21)$$

17

MICROSCOPE LAMP

```
┌──────────┐   ┌──────────┐   ┌──────────┐   ┌──────────┐
│ FND 100  │   │AMPLIFIER │   │ SPECTRUM │   │ PLOTTER  │
│ DETECTOR │───│   40 dB  │───│ ANALYZER │───│          │
│ BW = 350 MHz │              │          │   │          │
└──────────┘   └──────────┘   └──────────┘   └──────────┘

┌──────────┐   ┌──────────┐
│ LAMP     │   │ VARIAC   │
│ POWER    │───│0 - 140 V AC│
│ SUPPLY   │   │          │
└──────────┘   └──────────┘
```

FIG.II-3. Schematic drawing of experimental apparatus used for
shot-noise measurement of white light for the detector-
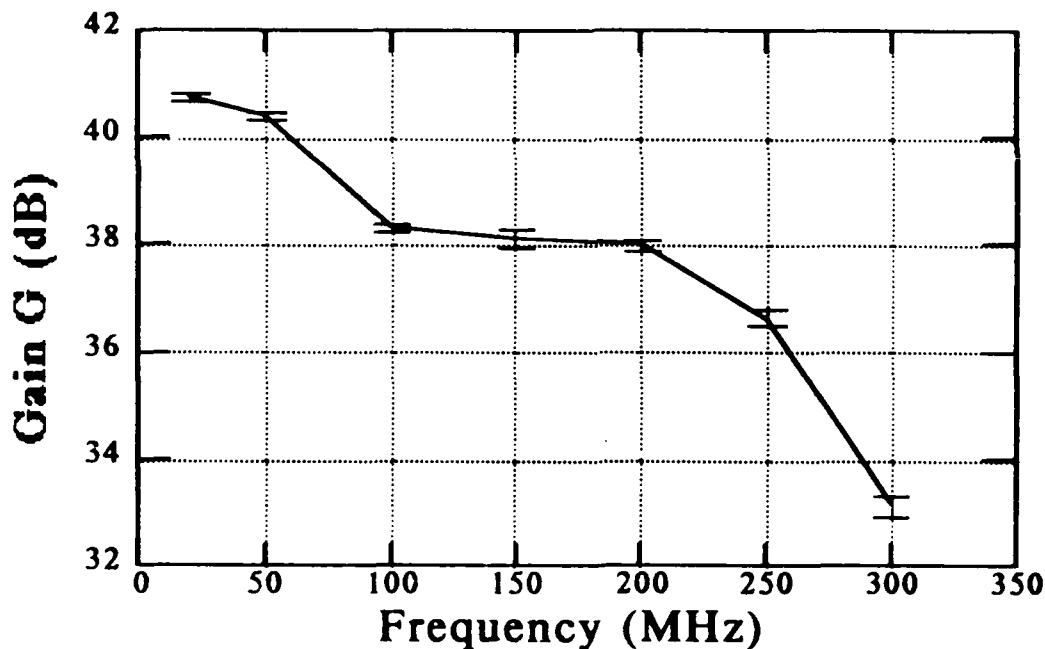amplifier gain calibration. The detector is from EG&G
Inc.

FIG.II-4. The detector-amplifier gain as a function of modulation
frequency calculated from the shot-noise measurement of
white light. The error bars represent the standard
deviation of ten sets of data.

where $P_{n,shot}$(calc) is given by equation (8) when G = 1.   The
determination of G has been carried out for 10 different power
levels and the result with error bars is given in figure II-4.

6.   DATA ON LASER GEOMETRY AND CHARACTERIZATION

The lasers used were a Spectra Diode SDL 2460 10-element
gain-guided laser array (fig.II-5a) and a 10-element index-guided
laser array with an anti-guiding geometry (fig.II-6a) supplied by
Dr. Botez of TRW.   The Spectra Diode laser array had an
individual stripe width of 10μm and gave a CW output power of 200
mW.   It had a relaxation oscillation frequency between 2 GHz and
3 GHz.   The detailed characteristics supplied by the manufacturer
are given in Table II.

Table II: Characteristics of Spectra Diode laser array.

Laser: SDL 2460
Manufacturer: Spectra Diode Labs, Inc.

Parameter	Pulsed	C	Units
threshold	184	188	mA
diff.Q.E.	59	54	%
slope eff.	.9	.83	W/A
V at 100mA	1.71	1.66	volts
resistance	1.49	1.00	ohms
I at 200mA	407	430	mA

test temperature: 25 deg. C
pulse: width = 200nsec, rate = 10kHz
wave length: 810 nm

TRW laser had an anti-guided array structure fabricated by
a two step metalorganic chemical vapor deposition growth [3].
According to Dr. Botez the fabrication procedure and the
characteristics of the TRW laser are similar to those given in
reference III-4.

The output power-current characteristics of the lasers are
given in figures II-5c and II-6c.   The far field of the Spectra
diode laser had two lobes (fig.II-5b) and that of the TRW laser
has (predominantly) only one lobe (fig.II-6b).

7.   REFERENCES FOR SECTION II

1. Amnon Yariv, "Optical Electronics", Holt Rinehart, Winston,
New York (1985)

2. K. Petermann, "Laser Diode Modulation and Noise", Kluwer
Academic Publishers, MA   (1988)
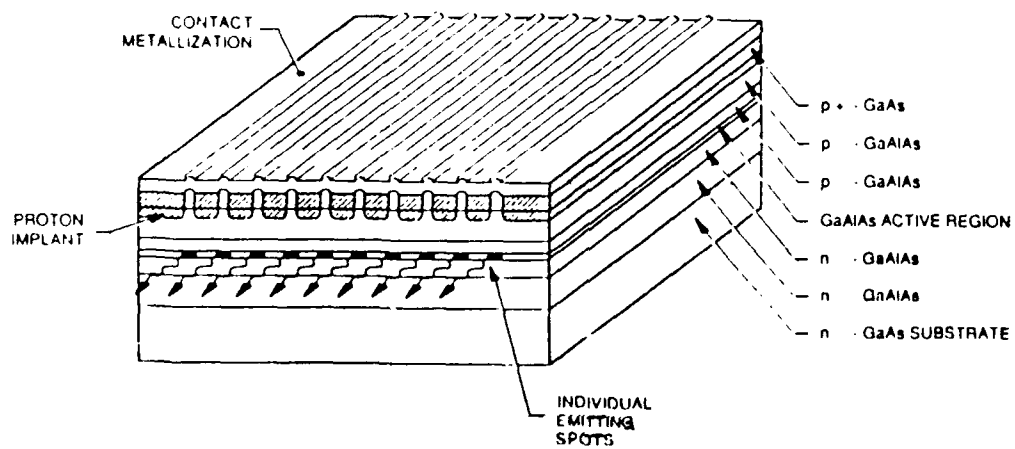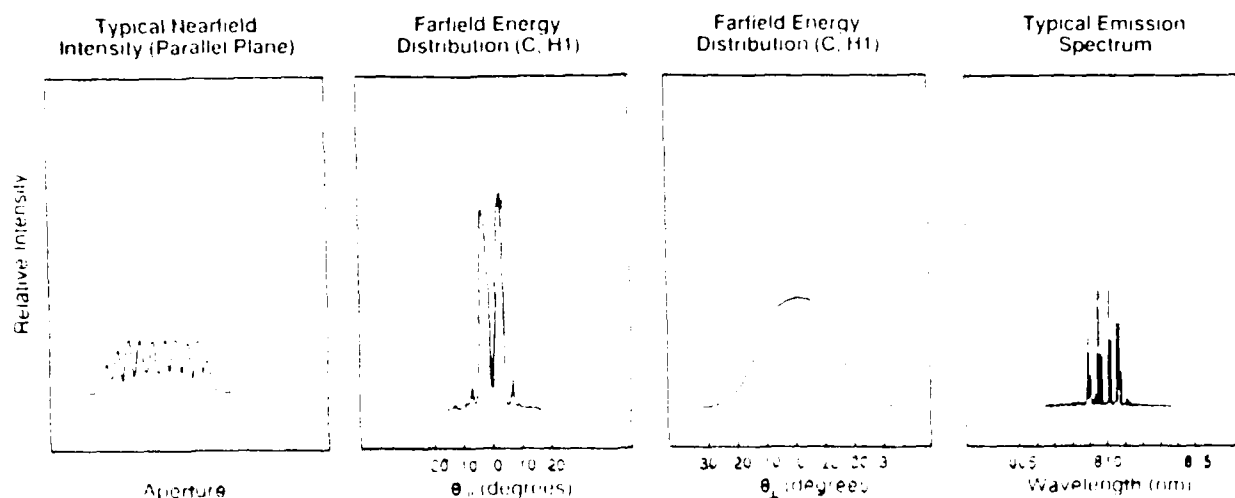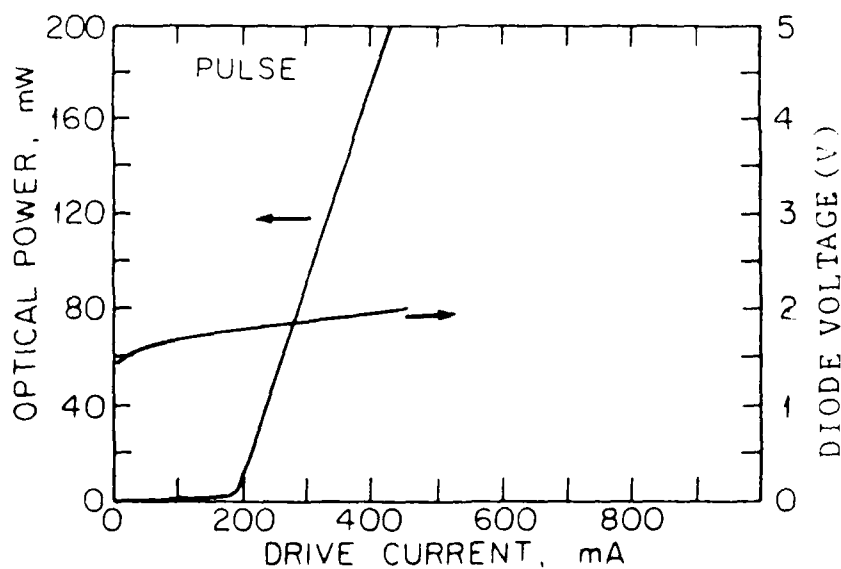
CONTACT METALLIZATION

PROTON IMPLANT

p + · GaAs
p · GaAlAs
p · GaAlAs
GaAlAs ACTIVE REGION
n · GaAlAs
n · GnAlAs
n · GaAs SUBSTRATE

INDIVIDUAL EMITTING SPOTS

FIG.II-5(a). The multi-stripe geometry of the ten-element gain-guided array.

20

| Typical Nearfield Intensity (Parallel Plane) | Farfield Energy Distribution (C, H1) | Farfield Energy Distribution (C, H1) | Typical Emission Spectrum |

(b)

(c)

FIG. II-5(b&c). The characteristics of the gain guided array from specifications supplied by the manufacturer: (b) the emission characteristics and (c) The variation of the output power and the junction voltage as a function of bias current.

21

1.0 μm

p GaAs (0 2 μm)
p GaAs (0 6 μm)
p Al₀.₄₀Ga₀.₆₀As (0 3 μm)
p Al₀.₁₈Ga₀.₈₂As (0 3 μm)
p Al₀.₄₀Ga₀.₆₀As (0 1 μm)

TRANSVERSE
OPTICAL
FIELD
OPTICAL MODE
n Al₀.₄₀Ga₀.₆₀As (1 25 μm)
SCH 5 QWELL ACTIVE
l_z = 80Å
l_b = 100Å
l_{conf} = 1000Å

n GaAs BUFFER (0 50 μm)

n GaAs SUBSTRATE

a.

b.

1.4 I_{th}

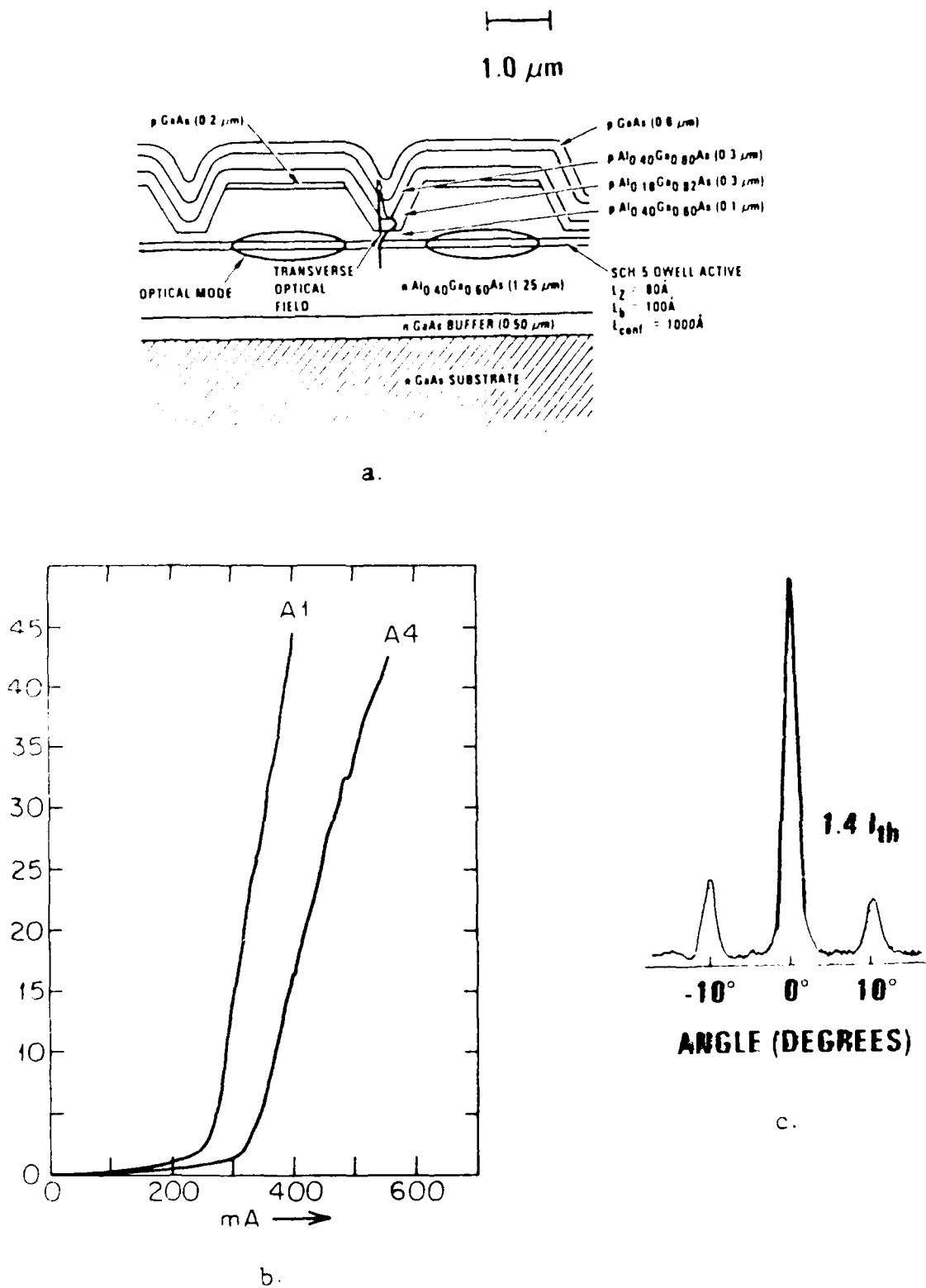-10°   0°   10°

ANGLE (DEGREES)

c.

FIG.II-6. Characteristics of antiguided array. (a) Schematic
cross section (there are ten elements), (b) emission
characteristics, (c) power output as a function of
drive current. (The noise measurements were performed
only on the A4 laser.)

3. L.J.Mawst, D, Botez, T.J.Roth, and G.Peterson "High power, in-phase-mode operation from resonant phase-locked arrays of antiguided diode lasers", Appl. Phys. Lett. $\underline{55}$(1), 10 (1989)

III. RESULTS OF MEASUREMENTS

1. RESULTS ON THE GAIN-GUIDED LASER

The RIN, measured as a function of bias current, is shown in Figure III-1. The RIN is maximum at threshold, similar to the behavior of single element lasers (Fig.III-2). As the bias current increases the RIN decreases rapidly and settles to a value greater than 20 dB lower than the peak value. This behavior is also similar to that of single element lasers.

It has been shown that for single element lasers, the RIN can be written as [1]

$$RIN \quad \alpha \quad [(I_b/I_{th}) - 1]^{-3} \tag{22}$$

for sufficiently large bias current I_b compared to the threshold current I_{th}. The RIN characteristics of most of the single longitudinal mode index-guiding lasers have similar noise levels at the same normalized injection current irrespective of the laser structure (Fig.III-2 a, b, c, and d). While gain-guided lasers exhibit a lower value of RIN at threshold, the RIN variation as a function of normalized bias current is relatively flat and smooth compared to the RIN variation of index-guided structures. Thus, far above threshold, index-guided lasers have smaller RIN than gain guided structures.

The results for the gain-guided Spectra Diode laser array show a 5 to 10 dB larger noise at threshold compared to both index-guided and the gain-guided single-element lasers. However, for higher bias currents, the RIN of the array is similar to the RIN of a single-element gain-guided laser (Fig.III-2f). At higher bias currents the RIN of both the gain-guided single element and array are much higher than the index-guided single-element lasers. Also, it is apparent that the RIN of the gain-guided array decreases much more strongly with current above threshold than does the gain-guided single-element lasers. However, at high bias currents RIN in arrays is independent of bias current as are gain-guided lasers. We conclude the following

1. The RIN of the array at threshold has a higher value (7 to 17 dB higher) compared to the RIN of both index guided and gain-guided single element lasers, at threshold.

2. The strong decrease with RIN just above threshold is

23

similar to the behavior of the index-guided single-
element lasers (Fig. III-2 a, b, c and d) and not
similar to the gain-guided lasers, which do not show a
pronounced peak at threshold.

3. The behavior of arrays at higher bias currents is
    similar to that of gain-guided single element lasers.
    That is, the RIN it becomes essentially independent of
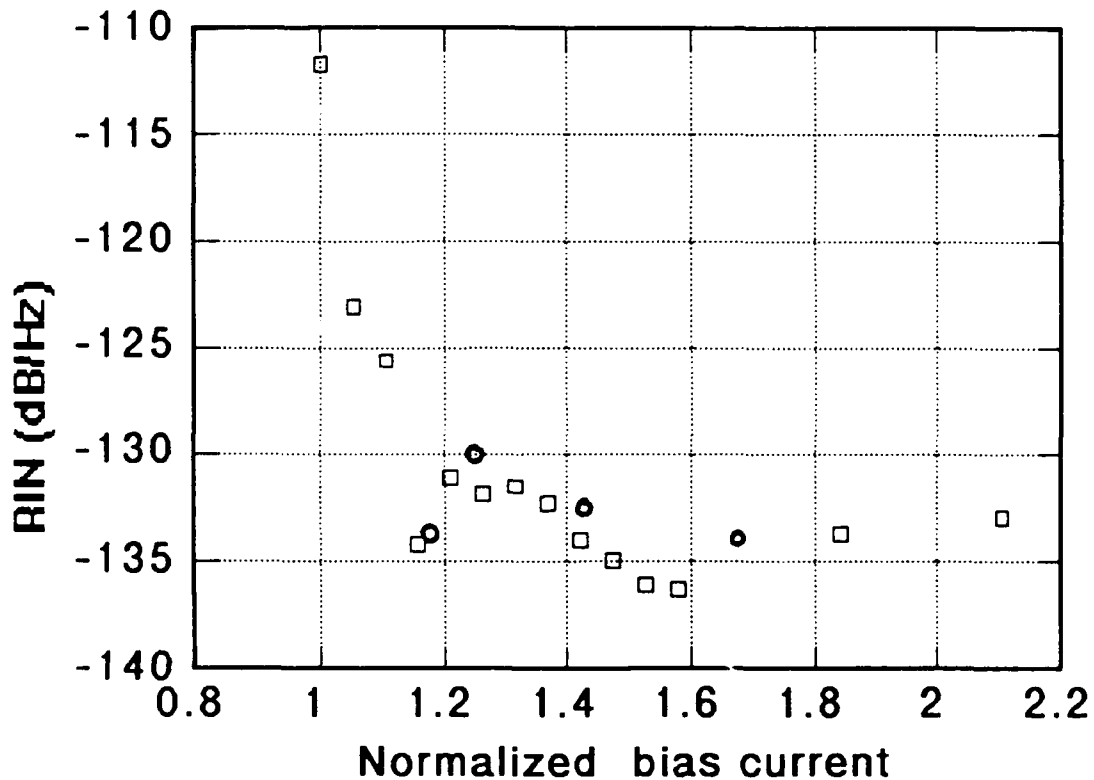

FIG.III-1. relative intensity noise versus normalized bias
          current (measured at 100 MHz) of the gain-guided
          array. Circled points represent data taken on
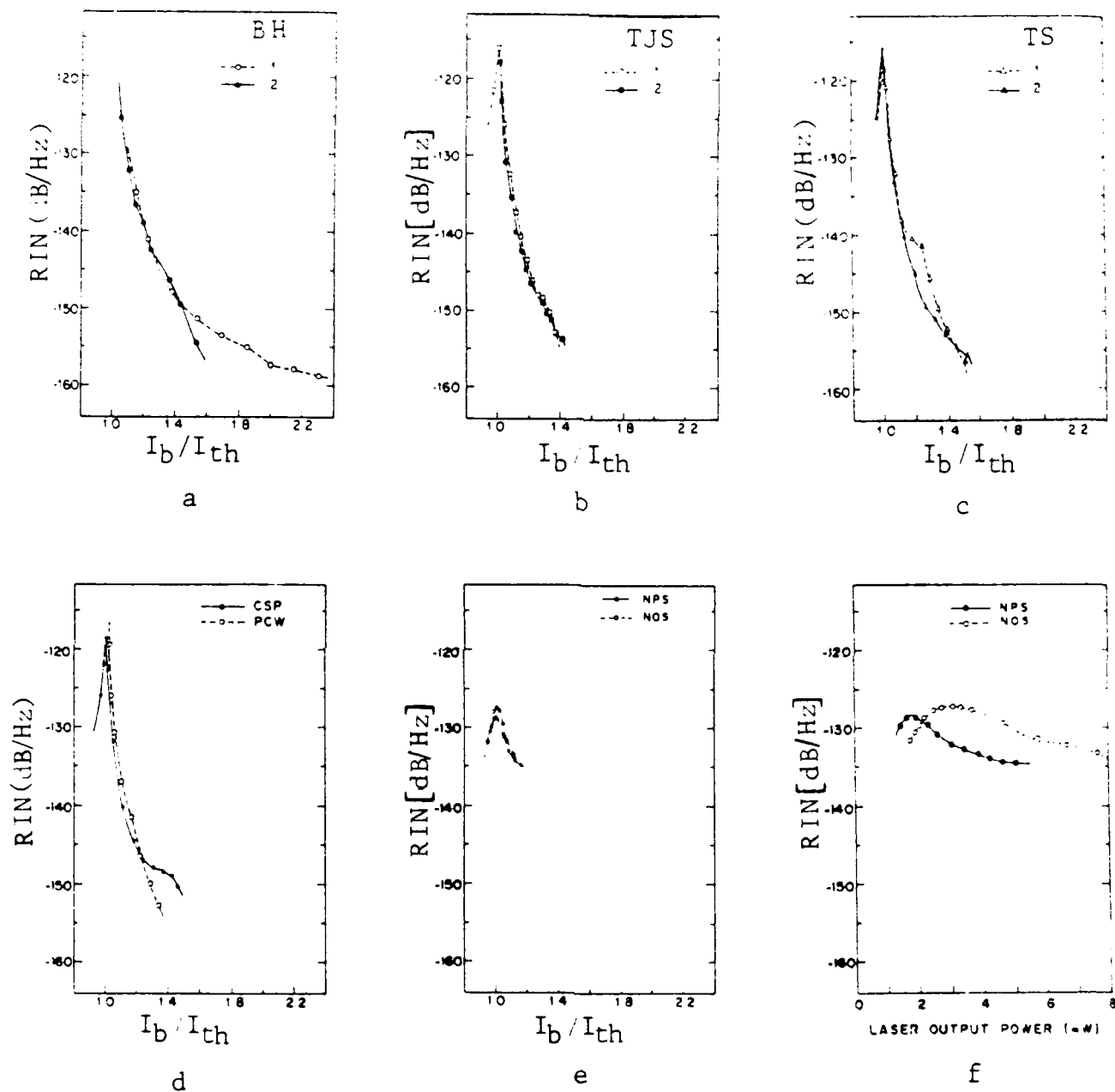   a different day.

FIG.III-2. **Relative intensity noise at 100 MHz versus normalized bias current reported for single element diodes: (a) buried-heterostructure (BH), (b) transverse-junction-stripe (TJS), (c) terraced-substrate (TS), (d) channeled-substrate-planar (CSP) and plano-convex waveguide (PCW), (e) narrow-planar stripe (NPS) and native-oxide-stripe (NOS) lasers, and RIN verses laser output for (f) NPS and NOS lasers (after ref. 1).**

drive current.

2. RESULTS OF INDEX ANTI-GUIDED LASER

The RIN measured as a function of bias currents for the TRW laser is given in Fig.III-3 . The following observations can be made:

1. The peak in RIN at threshold is similar to that of index guiding structures, as well as the absolute value of RIN near threshold.

2. The flattening of RIN with higher drive current and the absolute value of RIN at higher values of bias currents are similar to that of gain-guided structures, and not index guided structures.

Thus the arrays behave more like index-guided lasers at threshold, where they presumably operate single mode and more like gain-guided lasers at greater values of bias currents, where mode competition is likely to occur.

3. REDUCTION OF RIN WITH MODULATION

We have studied the modulation dependence of the relative intensity noise for the arrays, with measurements of the noise floor near 100 MHz. Two cases were considered, modulation at low frequencies (10 MHz) and modulation at 100 MHz, near the frequency of measurement.

Figure III-4 shows the noise floor in the TRW laser, modulated at 100 MHz, for various bias currents and modulation powers. At the modulation frequency and its multiples the signal is off-scale. However, between the modulation frequency components, it can be seen that the noise floor changes with increasing modulation depth. Near threshold the noise floor is increased by modulation. As the bias current is increased, the noise is reduced by modulation. Finally, at highest currents, no effect on the noise floor is seen due to modulation. Thus, there are apparently particular operating conditions for which modulation has the biggest effect on decreasing the noise floor.

Figure III-5a shows the noise floor for the SDL array as a function of frequency, modulated at 100 MHz. In this array, modulated at 100 MHz, it can be seen that it depends on the measurement frequency whether the noise floor is increased or decreased below the un-modulated case. In particular, at frequencies below 100 MHz the noise is decreased with increasing modulation strength, while at frequencies above 200 MHz the noise is increased with increasing modulation strength. As yet, we have no theoretical understanding for why there are different behaviors at different measurement frequencies.
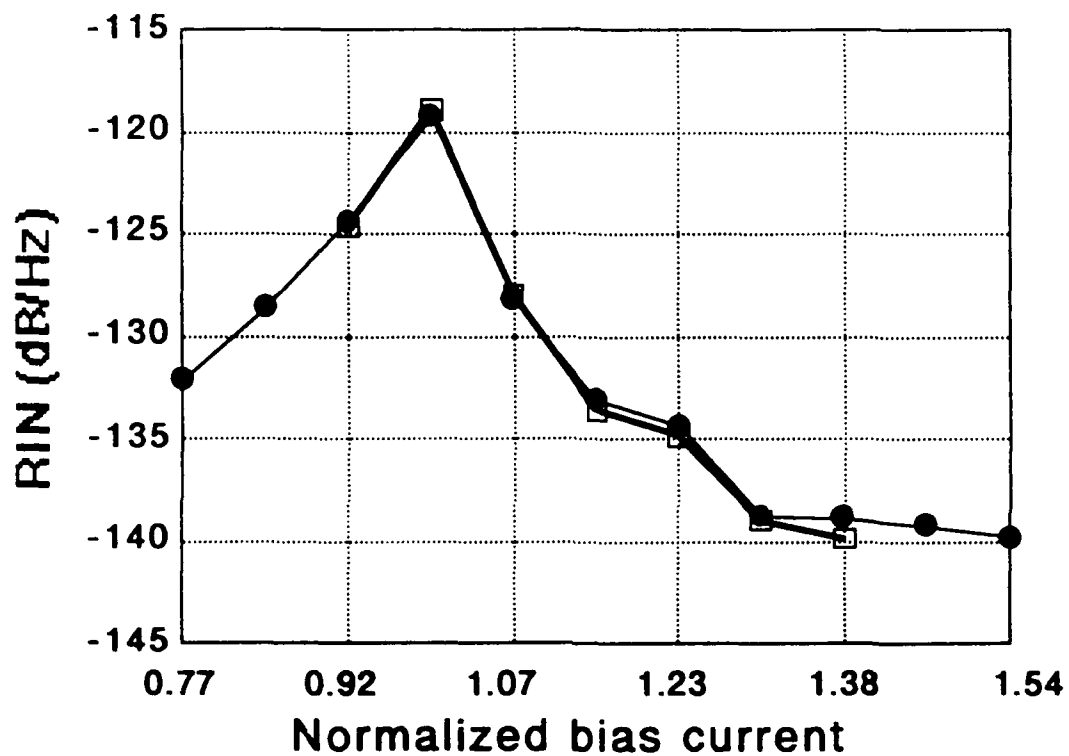
26

FIG.III-3. Relative intensity noise of index antiguided array as
a function of normalized bias current measured at 20
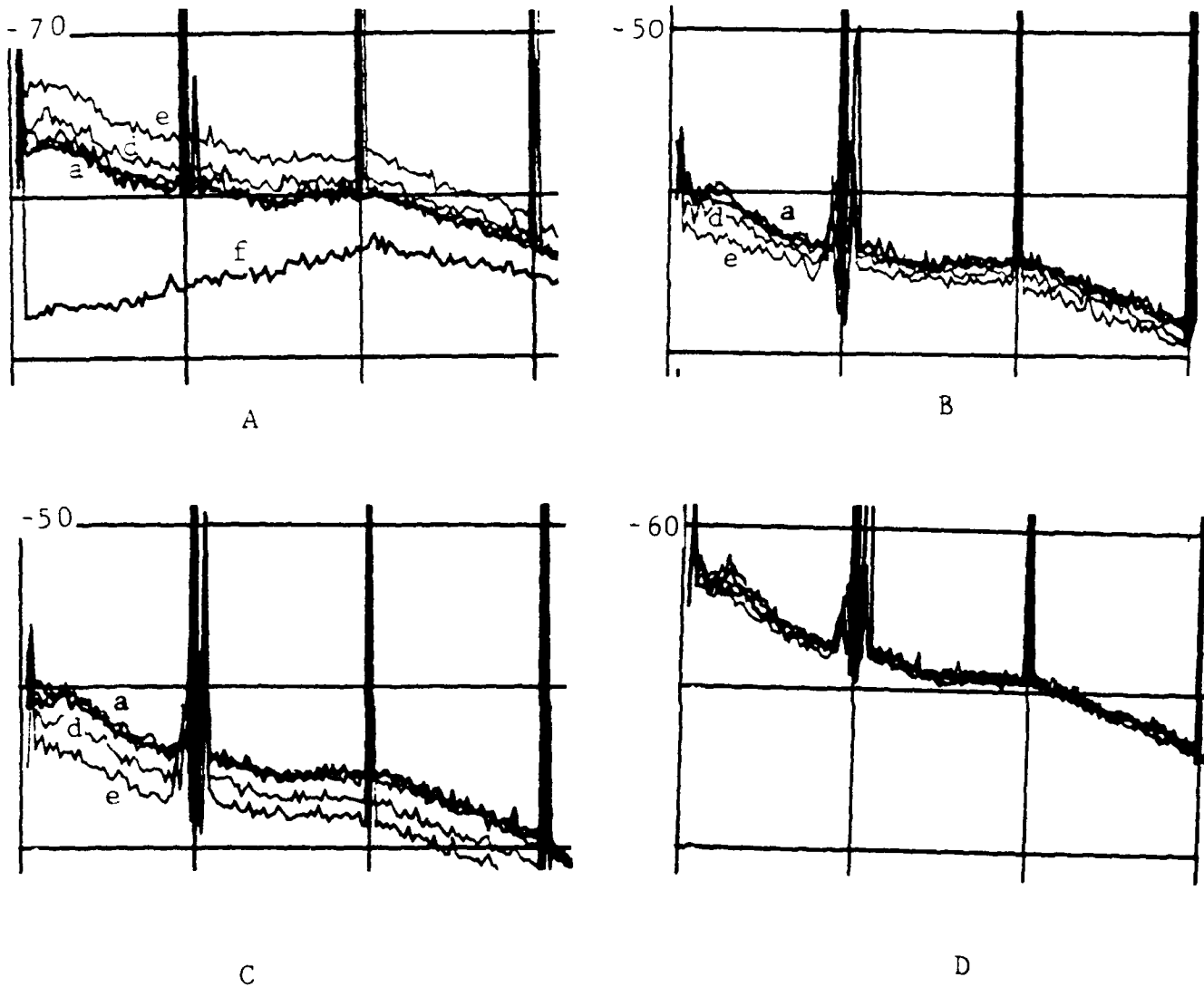MHz (two sets of data measured on defferent days).

FIG. III-4. Relevant portion of the spectrum analyzer display of
the output of the antiguide array in the presence of modulation
at 100 MHz at bias currents (A) 300 mA, (B) 350 mA, (C) 400 mA
and (D) 450 mA. (a), (b), (c), (d) and (e) represent noise floor
of the spectra with modulation powers 0, 1 mW, 3 mW, 10 mW and
31.6 mW respectively and (f) is the background noise. There are
a number of off-scale harmonics of the modulating frequency
present due to the gain saturation of the amplifier. Spectrum
analyzer band width = 100 kHz, vertical axis scale = 10 dBm/div,
horizontal axis scale = 100 MHz/div. Reference levels are marked
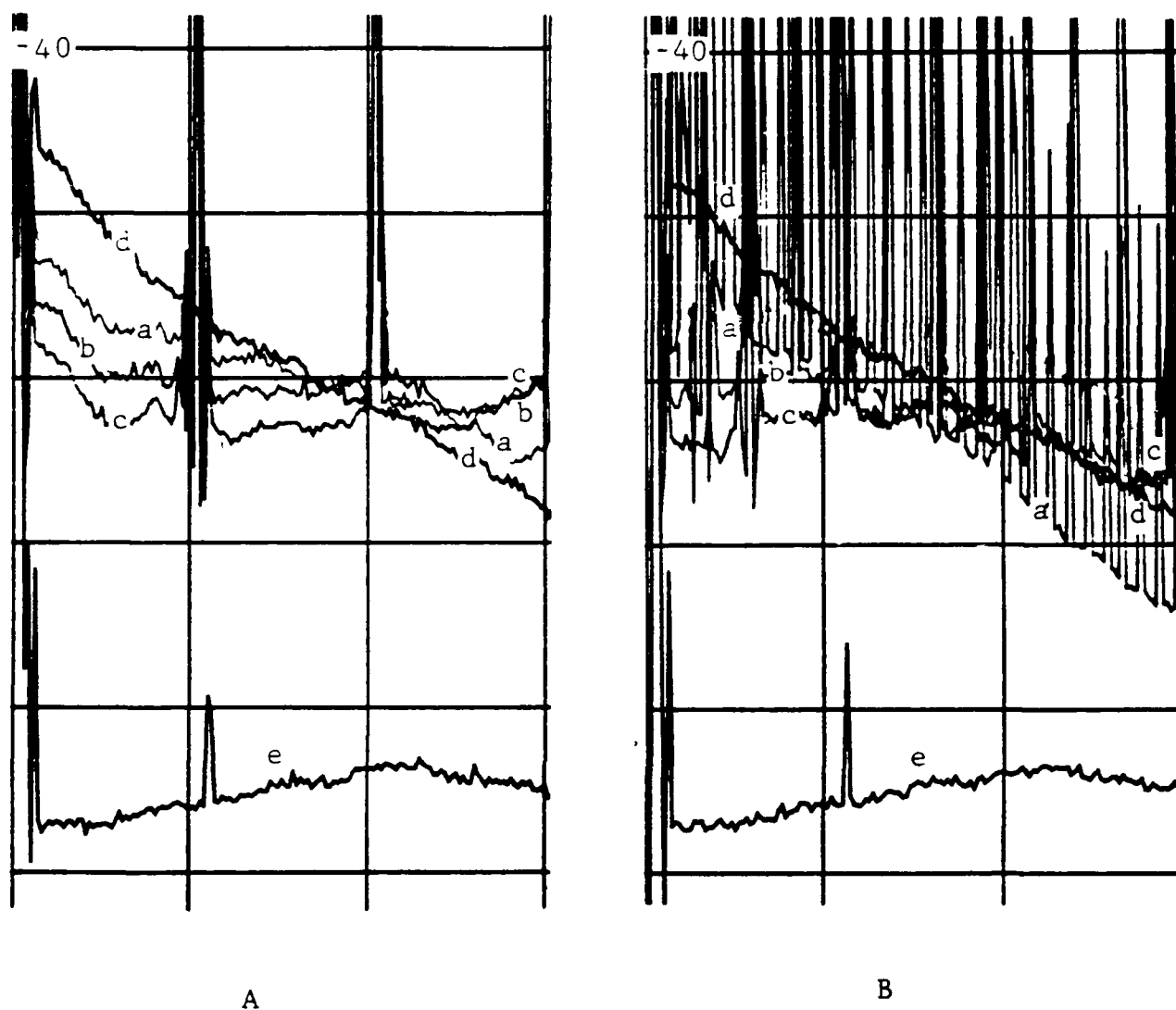in the figures.

A

B

FIG. III-5. Portions of the spectrum analyzer display of the
output of the gain-guided array in the presence of modulation
with bias current = 300 mA and detector current = 1.94 mA for (A)
modulation (with 31 mW of power) frequencies of (a) 10 MHz, (b)
26 MHz and (c) 52 MHz and for (b) modulation (at 100 MHz) powers
9f (a) 5 mW, (b) 10 mW and (c) 31 mW. (d) is the unmodulated
signal with (e) the background noise for both (A) and (B). All
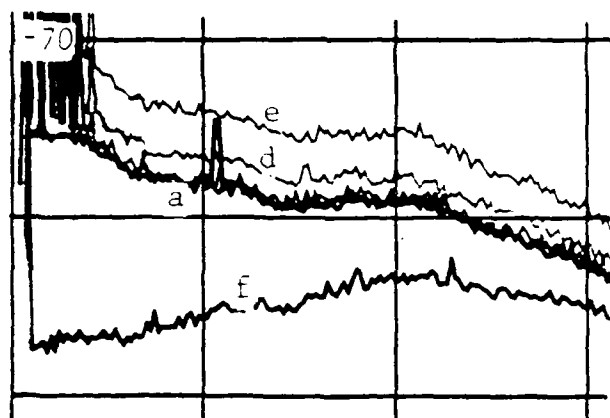other details are as given in Fig. III-4.

Figure III-5b shows the noise floor for the SDL array, for different modulation frequencies. It can be seen that as the frequency of modulation decreases, the behavior of the modulated noise floor relative to the unmodulated noise floor changes. In particular, when modulation is at 10 MHz, the noise floor reduction is independent of the frequency of the measurement. This means that at highest frequencies, the maximum noise reduction is with 10 MHz modulation, while at low frequencies the maximum noise-reduction is with higher modulation frequencies. The low-frequency modulation case was studied carefully and data are presented in Figures III-6 and 7. Again, we do not yet have a theoretical model for these results.

Figure III-6 shows the TRW array modulated at 10 MHz. It can be seen that the noise reduction is independent of measurement frequency, but depends on both the bias current and the modulation power. Figure III-7 shows the SDL array, also modulated at 10 MHz. The results are similar to that of Figure III-4. That is, maximum noise reduction occurs for a particular bias current and a particular modulation power. The rate equations must be solved in the simultaneous presence of a modulation signal and a noise signal to model these results. It is expected that the reason for this complicated behaviour is the nonlinear interaction between the photon field and the carrier dynamics in the semiconductor laser.

From the data in the previous four figures, it is possible to plot the noise floor as a function of modulation power for a given physical situation. Two examples are shown in Figure III-8, one for the TRW array and one for the SDL array.

The Relative Intensity Noise is always lowest at higher bias currents. Thus, for low-noise operation, it is most important to look at the effect of modulation at higher bias currents. For the Spectra Diode array we measured (at higher bias currents) the noise to be minimum for a modulation index m - 0.2 (which correspond to a modulation power - 10 mW). At higher modulation index the RIN slightly increases. The results for the TRW array are similar to that of the Spectra Diode Array for higher bias currents. Maximum RIN reduction (about 18 dB) was observed near the threshold bias currents (It = 325 mA), because the average laser power increased with modulation strength. For bias currents greater than the threshold values, a maximum reduction of 7-10 B was observed for both the lasers.

Previous measurements were made in an external-cavity laser, with modulation at frequencies larger than the measurement frequency [1], and a 25 dB reduction in noise with increasing modulation power was observed. With single-mode BH and TJS single-element lasers, when both modulation and measurement were near 100 MHz, very little affect was observed in the noise floor
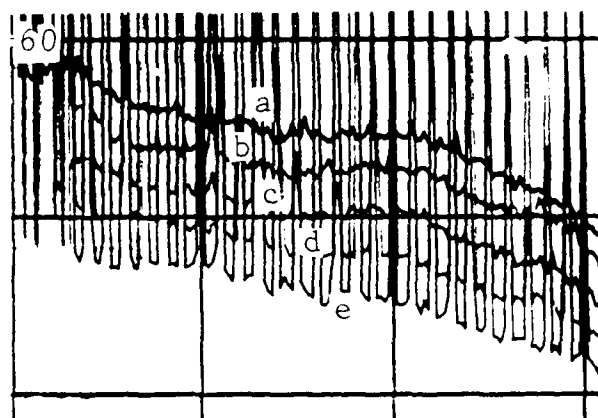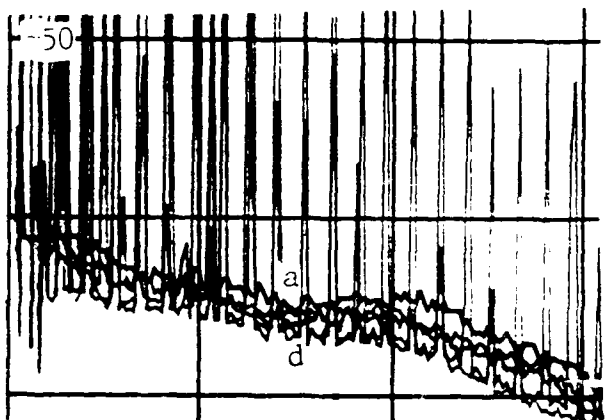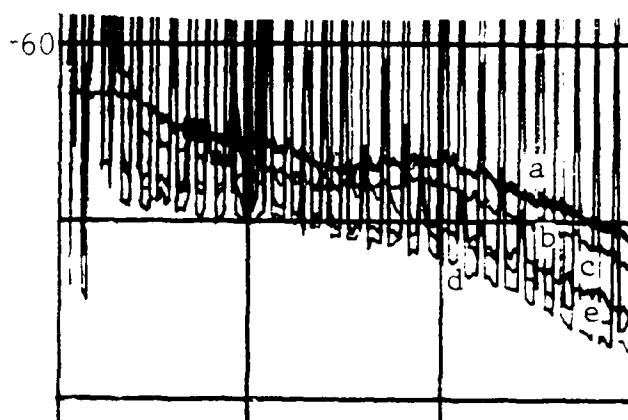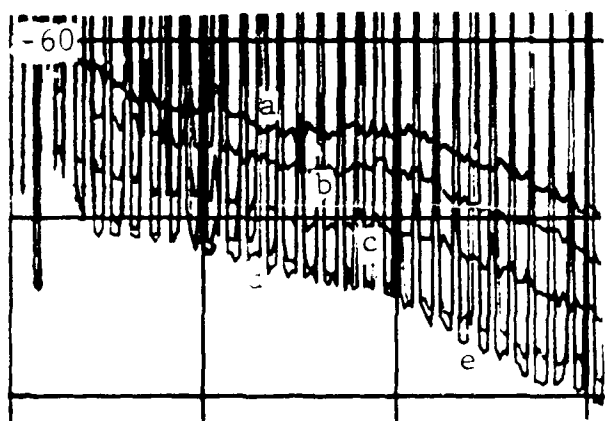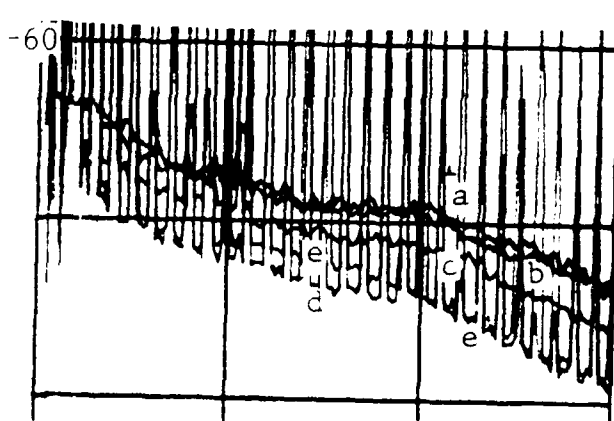
FIG. III-6. Portion of spectrum analyzer display of the output of the antiguide array with modulation at 10 MHz frequency with bias currents (A) 300 mA, (B) 325 mA, (C) 350 mA, (D) 375 mA, (E) 400 mA, and (f) 450 mA. Other details are as given in Fig. III-4
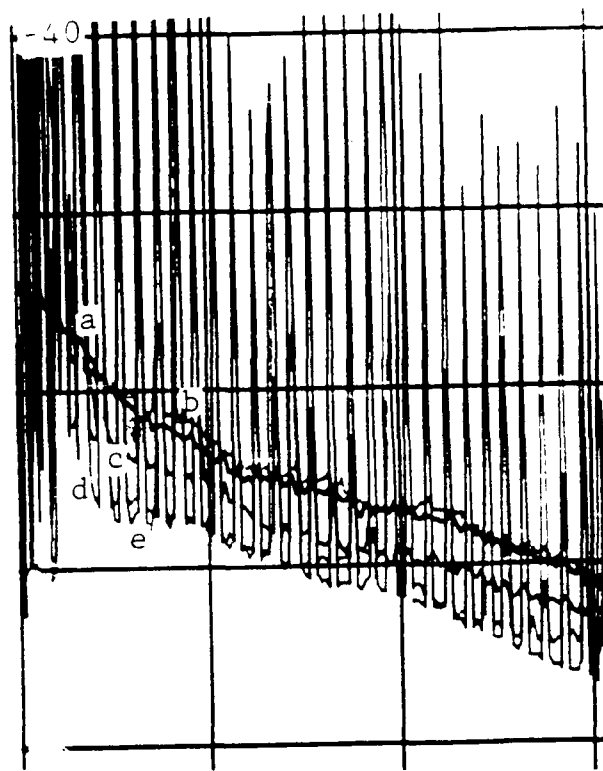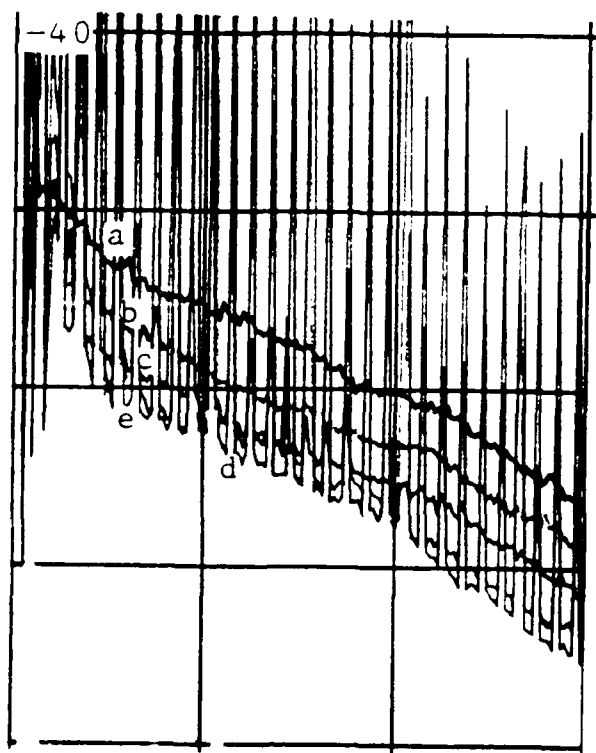
FIG. III-7. A,B,& C. Portion of
the spectrum analyzer display cf
the output of the gain-guided
array with modulation at 10 MHz
for bias currents (A) 200 mA,
(B) 225 mA, and (C) 250 mA.
Other details as same as given
in Fig. III-4.

D

E

F
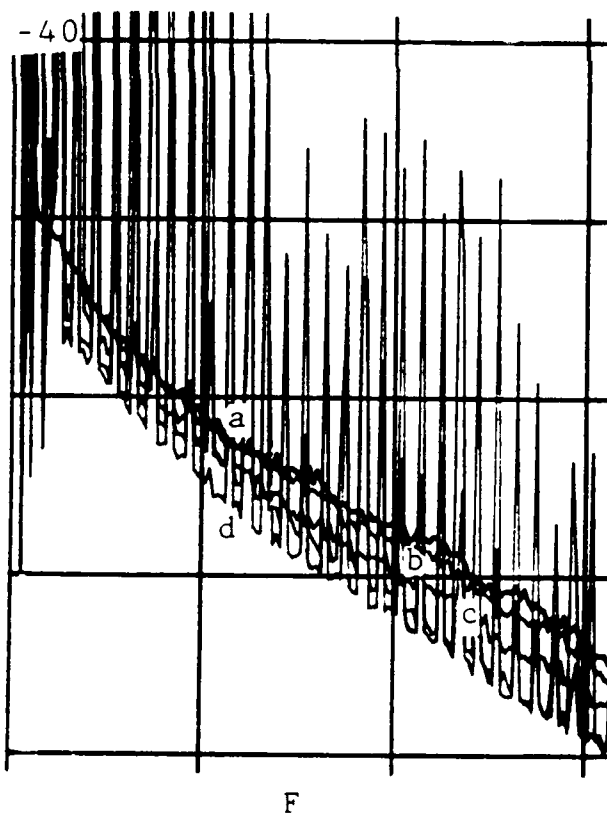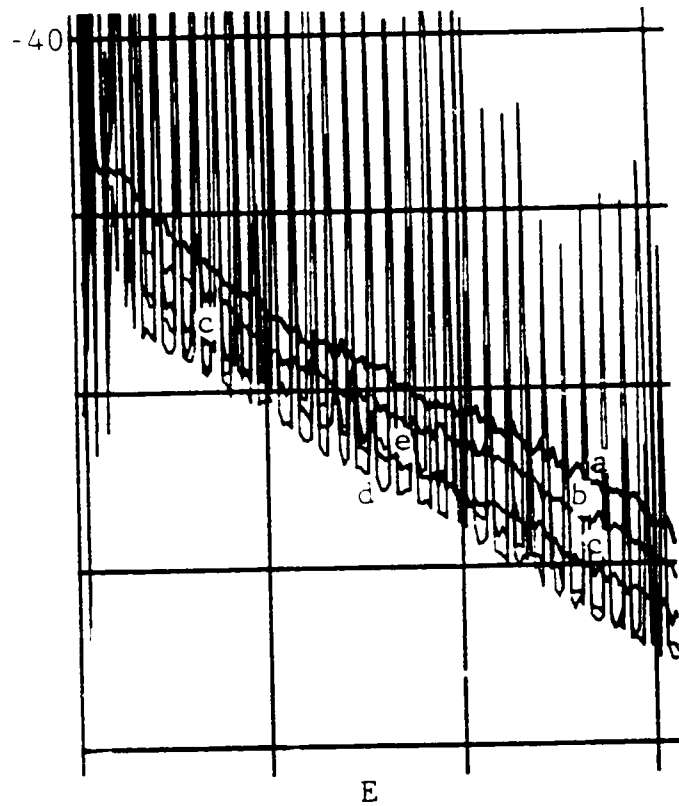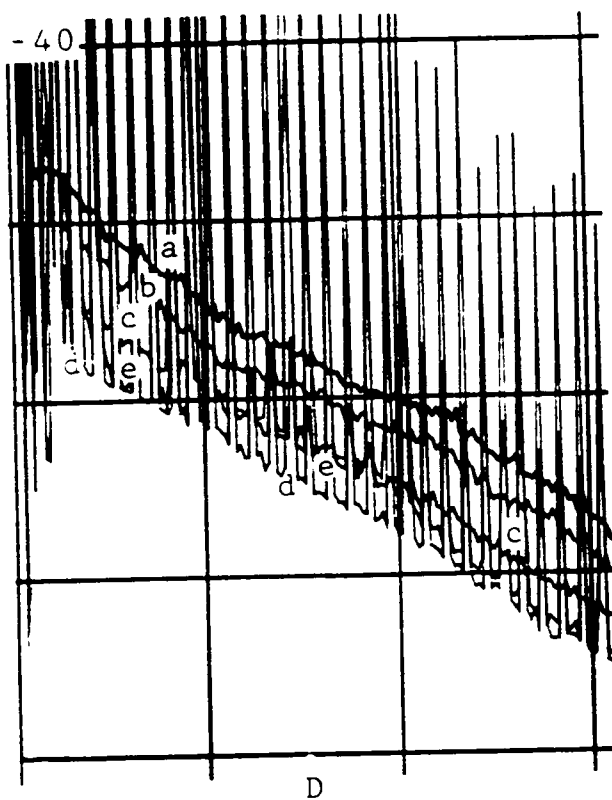
Fig. III-7 D,E,& F. Portions of the spectrum analyzer display of the output of the gain-guided array with modulation at 10 MHz for bias currents (D) 275 mA, (E) 300 mA and (F) 325 m. Other details are as same as given in Fig. III-4.
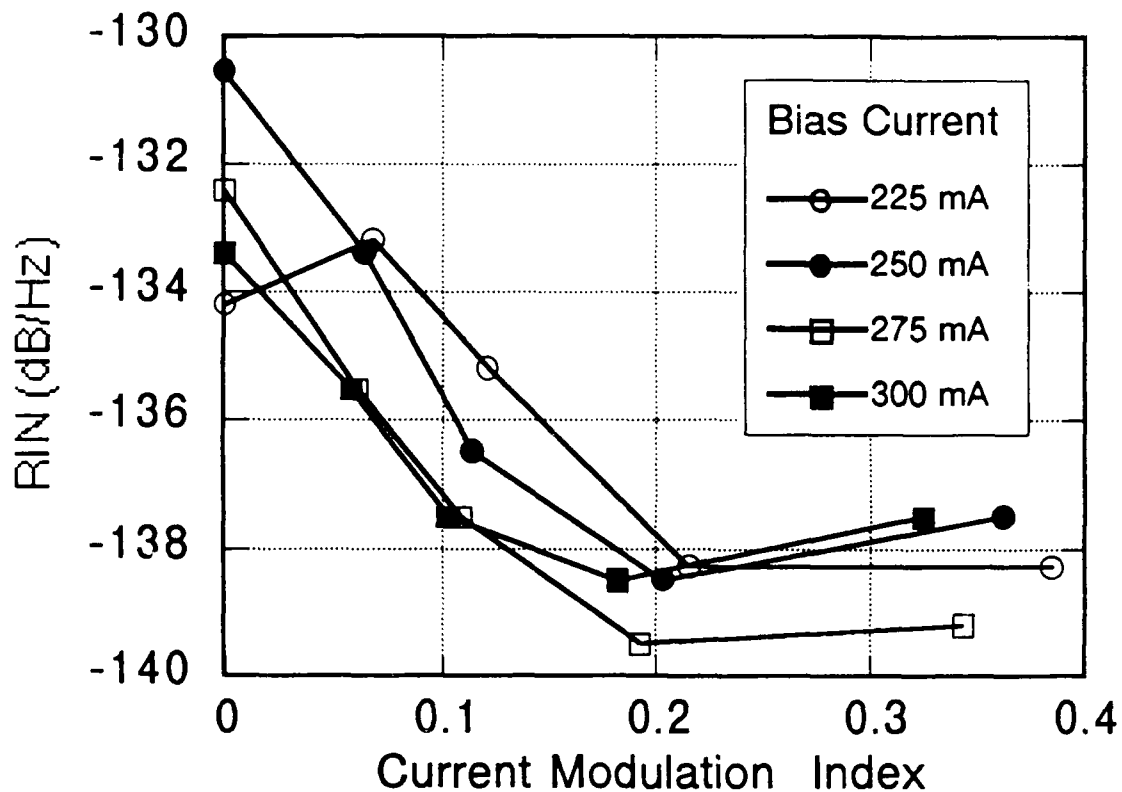
FIG.III-8a. Effect of modulation (at 10 MHz) on RIN for gain-
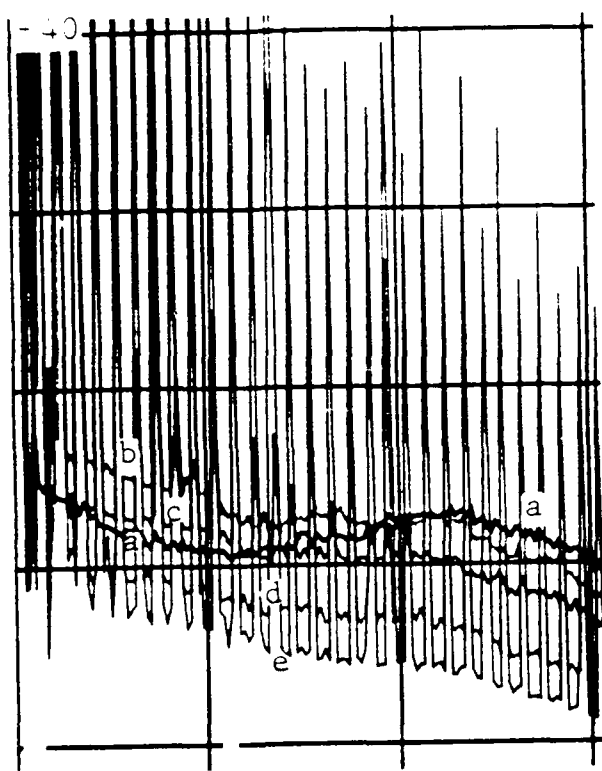guided array for different bias currents. The
measurement frequency is 100 MHz. Since there was a
strong harmonic of the modulating frequency present
at 100 MHz (and all the other multiples of the
modulating frequency) in the noise spectrum, the
measurement of noise at 100 MHz was not possible and
hence an average of the noise measured at 95 MHz
and 105 MHz was treated as the noise at 100 MHz.
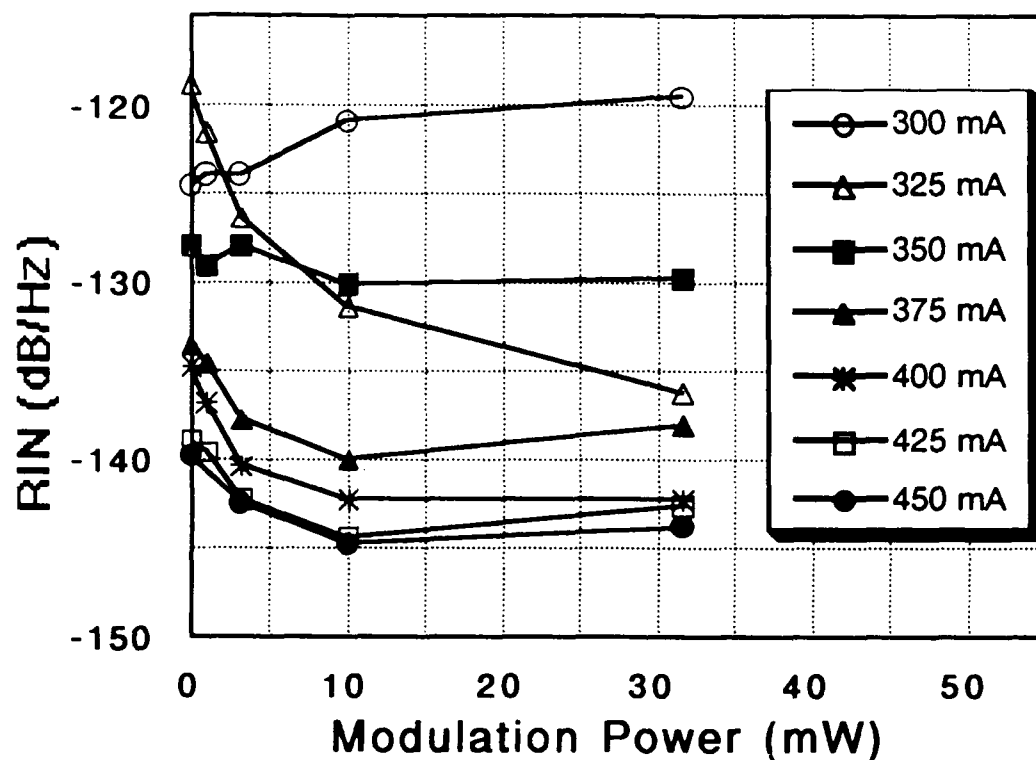
FIG.III-8b. RIN of index antiguided laser as a function of
electrical modulation (at 10 MHz) power for various
bias currents. The noise was calculated for 30 MHz.
(An average of the noise at 25 MHz and 35
MHz was computed as the noise at 30 MHz.)

35

with increasing modulation index (as long as it was under 0.5) [2]. Increased modulation index increased the noise floor.

What is needed is a systematic study of the affect of modulation on the noise floor. This study should be experimental, with theoretical back-up for an understanding of the effects.

4. REFERENCES FOR SECTION III.

1.. Kristian E. Stubkjaer and Martin B. Small, "Noise properties of semiconductor lasers due to optical feedback", IEEE J. Quantum Electron., vol. QE-20, pp 472-478, May 1984.

2. Ken-ichi Sato, "Intensity noise of semiconductor laser diodes in fiber optic analog video transmission" IEEE J.Quantum Electron., vol. QE-19, pp.1380-1391, September 1983.

IV. THEORETICAL INVESTIGATION OF NOISE DUE TO MODE-COMPETETION

IN GAIN GUIDED SEMICONDUCTOR LASER ARRAYS

This section reports a numerical analysis of transient turn-on in a gain-guided semiconductor laser array. The self-consistent approach, valid in the strong-coupling limit, treats the array as a single waveguide laser with transversely varying refractive index. This model makes clear how mode competition occurs in gain-guided laser arrays, and leads to noisy output at certain current levels.

A. Introduction

Transverse mode-competition has been investigated since the early days of lasers [1]. Unstable laser output due to this effect has been more recently demonstrated both theoretically and experimentally in solid state (neodymium) lasers [2], HF chemical lasers [3] and CO_2 lasers [4,5]. In the first case, the situation is similar to the one present in semiconductor laser arrays, the difference being that the transverse modes are not shaped by waveguiding (either gain or index -induced) but by diffraction at the resonator aperture and the limits of the active medium rod. In CO_2 lasers, chaotic behavior was observed under some circumstances, but the results cannot be extrapolated to semiconductor lasers in any way, since in the transverse mode competition problem in this laser, not only the gain distribution in the transverse direction and its hole-burning effect are important, but also the inhomogeneous heating of the gas, giving rise to self-defocusing effects which modify the field distribution.

Some studies have been carried out on the nonlinear

36

interaction of the transverse field distributions in multi-stripe
laser arrays predicting stable, periodic and chaotic output
amplitude depending on the operation conditions [6,7]. Some
experiments carried out in gain-guided MQW laser arrays [8] and
Y-coupled laser arrays [9] seem to confirm the existence of
unstable output. However, the theoretical analysis has been
performed under the assumption of index-guiding structures, and
using the coupled-mode formalism. This approach has been
extensively used in the study of the dynamics of semiconductor
laser arrays [10], but in gain guided devices the interelement
coupling is strong and can affect nonadjacent elements, and a
representation of the field as a linear combination of the modes
of the isolated elements can be questioned. In particular, the
coupled-mode approach is probably inadequate to describe the
gain-guided array, since this structure only supports leaky
modes, where power freely flows in the interelement gaps and in
the substrate. Such modes cannot be adequately represented by a
field distribution obtained by combining individual modes of the
elements, coupled to each other by a small overlap [11]. The gain
guided array problem is important since gain guided laser arrays
are the ones commercially available at the present time.
Moreover, gain guided lasers are more sensitive than index guided
ones to nonlinear photon-carrier interactions, since the modal
field distribution is tailored by the gain distribution instead
of the refractive index. Hence, any variation in the gain
distribution will modify the field distribution in the array,
while a reciprocal interaction is induced by the stimulated
recombination process.

For these reasons, it is desirable to do an analysis of the
dynamic regime of semiconductor laser arrays based on the use of
the exact orthogonal eigenmodes of the whole array as a single
waveguiding structure, and taking into account the variation of
the modal field profiles with the variations in the gain
distribution. The purpose of this paper is to present a
simplified approach to this problem which provides an interesting
view on some mode competition problems arising during the
simulation of turn-on transients.

B. Approach

The self-consistent solution of the field-carrier
interaction in a semiconductor structure usually requires the
iterative solution of (i) Poisson's equation giving the current
distribution in the structure, (ii) the carrier distribution
induced by current injection and the lateral diffusion of charge,
and (iii) the field distribution obtained solving the wave
equation with the refractive index distribution induced by the
charge concentration [12]. Then photon-induced recombination must
be taken into account, and all the equations solved again for the
new conditions in an iterative way which will stop when a steady
solution is obtained. Some simplified approaches allow the

37

simultaneous solution of some of the equations rather than an iterative solution [13]. Usually the solution of the current distribution must be performed in a two-dimensional cross section, while both the charge and field distributions are considered one-dimensional problems by assuming that carriers are confined in the active layer, and using the effective-index aproximation [14,15]. The propagation direction is usually ignored, calculating an averaged photon-carrier distribution along the resonant cavity, as in [13]. More sophisticated models also consider the propagation direction by propagating a field along the resonant structure which becomes conformed by both the waveguide and the resonator in any round trip, rather than calculating the waveguide modes and ignoring the resonant cavity. Again a steady solution is reached after a great number of iterations [16]. This self-consistent method has been successfully applied to semiconductor laser arrays both using modal field solutions [17] and propagating beam modelling [18] in order to obtain field and gain distributions in the steady state. All of these self-consistent methods, however, are difficult to apply to dynamic problems, where the temporal impact of any iteration step should be quantified.

Our simplified approach uses a unidimensional model for the current and carrier distribution. The distributions are layered in regions under the gain elements where both current and carriers are assumed to be uniformly distributed, hence the refractive index is going to be constant. Here we present the simplest case in which the layers have been associated to the laser stripes and gaps. Of course more accurate results can be modelled by considering a higher number of layers per laser stripe with constant parameters in each layer. The field distribution is then calculated in the multilayer waveguide in a given simulation step in order to self-consistently determine the gain, photon distribution, and filling factors of all of the involved modes. With this data, the time-dependent photon-carrier interaction is calculated in short time intervals using the rate equations (averaged over the length of the laser). The transient turn-on of a four-element gain-guided array is calculated as an example.

C. Refractive Index Model of the Laser Array

In actual gain-guided semiconductor laser arrays, such as sketched in Fig. IV-1a, the current flux is favoured in certain regions (the laser "stripes") either by inducing high resistivity channels between them in the upper cladding, right below the ohmic contact, or by using multielement contacts separated by gaps where carriers are not injected. The optical field will present a two-dimensional cross-distribution profiled by both the composition of the different layers of the heterostructure, and the carrier distribution, which depends on the current flux distribution and the stimulated recombination. A basic assumption

38

of our analysis of such lasers is that the heterostructure will confine the generated carriers in a thin layer which will constitute the active region where the carrier-photon interaction is produced. All the other layers will be considered as passive regions where no light-matter interaction is observed other than a certain light scattering which introduces uniform losses.

The effective-index approximation is used, assuming that the optical field can be approximated by the product of two functions $A(x,y)\Phi(x)$. One of them, $A(x,y)$, will present a strong variation along the direction of crystal growth (labelled as the y in Fig.IV-1), and a very smooth variation along the layers [14,15]. Since the smooth variation along the active layer due to the carrier-induced modulation of the refractive index is small, its derivative can be neglected and $A(x,y)$ can be separately solved for. This function accounts for the field confinement within the thin active layer, which, in general, will present a single-lobe (fundamental mode) distribution. The other function, which only varies with x, will account for the variation of the field along the layers, representing the lateral confinement of the modes. The broad-area nature of multielement semiconductor phased laser arrays will allow, in general, the propagation of several field distributions along this direction, which defines the several transverse modes of the structure. It is this multimodal character which is the focus of this study. Hence, the the optical field distribution of interest is given by the unidimensional Helmholtz equation:

$$d^2\Phi/dx^2 + [k_o^2 n^2(x) - \beta^2]\Phi = 0 \qquad (1)$$

where n(x) is the (mode independent) effective-index distribution along the direction parallel to the active layer, k_o the vacuum propagation constant, $2\pi/\lambda$, and Φ is a one-dimensional function which accounts for the modal distribution along x. Since TE and TM modes are essentially degenerate, only the simpler TE solutions of equation (1) are considered, corresponding to light polarised along the axis of crystal growth (y).

The effective-index distribution along x is a set of one-dimensional layers, shown in Fig. IV-1b, corresponding to high-current stripes, of complex refractive index n_c, with gaps between stripes (which may also have some gain) of complex refractive index n_g, and the "substrate-like" external layers, where current flux is going to be approximated by zero (the refractive index, n_s, may still be complex because of possible losses). Since the interest is in the dynamic behavior of the "gain-guided" semiconductor laser arrays, not in the real field distributions of these devices, the model is as simple as possible to get a reasonable trade-off between computing efficiency and physical presentation of the dynamic effects. Thus it is assumed that any single layer will have a constant (x-independent) current flux and carrier density. Also, the current

39

flux is assumed to be constant in time (dc bias), and identical
for all of gain elements, while the current density in the gaps
is related to that in the gain elements by a fixed ratio:

$$r_J = J_{gap} / J_{laser\ element} \tag{2}$$

The injection of carriers in any of the layers will be
considered to depend only on the instantaneous current flux in
this layer. In this way the effective index distribution of
equation (1) becomes layered.
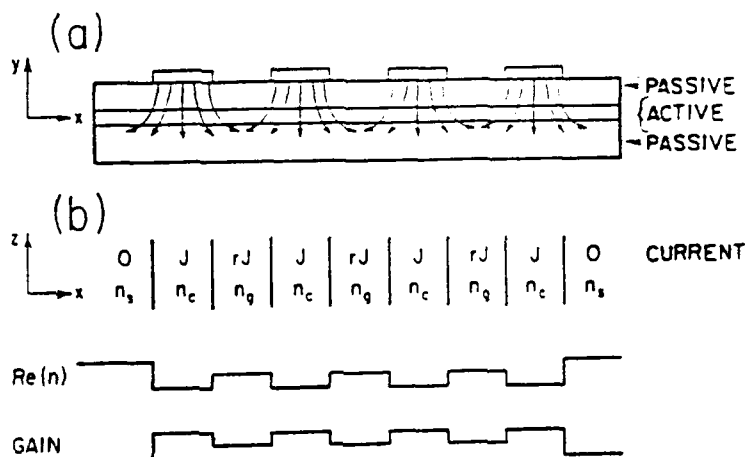
Figure 1. Diagram of gain-guided laser array before including
stimulated emission: a) geometry defining x and y axes, showing
current path; b) one-dimensional waveguide model, showing the
current and complex refractive index assumed in each layer. In
the presence of stimulated emission, each layer has a different
refractive index, n_j.

The effective index in the most external layers is called
the "substrate" effective index n_g, since this represents the
substrate of our equivalent multilayer one-dimensinal waveguide.
The effective index in any other layer, j, will depend on the
gain of this layer, which will be proportional to the carrier
density, as follows:

$$n_j = n_g - (R + i) \frac{a\ N_j}{k_o} \tag{3}$$

In this formula, a is the constant which relates the carrier
density in the layer N_j with the absolute gain per length unit, R

40

is the antiguiding parameter, and i the imaginary unit. The effective index method will predict a different confinement of the field within the active layer in regions with different refractive indices.

The imaginary part of the refractive index will vanish at the transparency threshold N_{tr}. Under normal operation, the array will have gain ($N>N_{tr}$) in certain regions which will constitute the laser elements, yet losses will be present in the gaps and will be maximum in the substrate. Due to the antiguiding effect of the gain, the refractive index will be maximum in the substrate, such that this structure will only support leaky modes. Then, energy exchange between the laser elements is not produced by waveguide coupling through evanescent waves, but is carried by travelling fields, such that the different gain elements in the gain guided laser arrays are locked in phase by the fundamental nature of the supported modes, more than by the degree of overlap of the local modes of isolated laser elements. It is this self phase-locking effect of antiguiding structures that has suggested the use of index-induced antiguide arrays for efficient coherent laser arrays [10,32-33].

Coupled-mode theory cannot be used in anti-guide situations, and an exact analysis is necessary by making use of the exact modal field distributions in the array considered as a single waveguiding structure. Since the number of leaky modes in a waveguide is infinite, the analysis of the laser problem must be limited to those modes whose induced gain is higher than the leaky losses. These modes are going to be different for any particular carrier distribution in our layered model, and the carrier distribution is also modified by stimulated recombination, which depends on the photon distribution of the involved modes. For this reason it is necessary to have an understanding of the possible involved modes, so that they can be easily found at any step of the simulation among all the infinite possible solutions of equation (1).

D. Modes in a typical four-stripe array

An example of the positive gain modes within a multilayered waveguide of the kind described above was calculated by using the scattering matrix method for multilayers [34,35,24]. The number of roots of the eigenvalues function can be reduced and the algebra simplified in the symmetrical case by solving the wave equation (1) in half the waveguide, so that the boundary condition for ϕ at the waveguide axis can be split into odd (zero value) and even (zero derivative) modes, which can be identified separately. The boundary condition in the external part will always be that the field amplitude cannot grow indefinitely in the substrate. For this calculation the bulk effective index is taken as 3.5 with effective losses on the order of 200 cm^{-1} at

820 nm; the laser elements were assumed to provide a gain of about 100 cm^{-1}. Actual complex indices were 3.5+0.0026i for the substrate, and 3.4883-0.0013 in the gain elements; i.e., the antiguiding parameter has been taken as 3. The refractive index in the gaps between laser elements was taken as 3.4952+0.001, so that the actual absolute gain above the losses is one third of that in the gain elements. A four stripe array with 5 micron wide stripes and 4 micron gaps has been assumed. Fig. IV-2 shows all but one of the modes which were calculated to have positive gain. Fig. IV-2a shows the only index-guided modes with positive (even though very small) gain. "Index-guided" means that the real part of the propagation constant is greater than the smallest of the refractive indices (which is that of the gain elements). Also shown in Fig. IV-2a are the real refractive index profile and the gain profile across the array. Because of symmetry, only half the full array is shown. It can be seen that these index-guided modes appear primarily between the stripes, but the gain is 0.092 cm^{-1}, which can be considered close to cutoff. Reflection losses will not allow their excitation.

The rest of figure 2 shows the gain-guided modes (real part of the propagation constant smaller than the substrate). The modes have been ordered by the real part of the propagation constant, so that Fig. IV-2b,c,d represent the half-distributions of the modes with one, two or three lobes in the gain elements. There is still one more mode with positive gain, but very small. It can be seen that these modes appear primarily under the stripes, in the location of the largest gain. In Fig. IV-2 the zero represents the waveguide axis, and the other half would be the mirror image of the represented part. Abscissae represent the distance normalized to the full width of the array.

E. <u>Dynamic Model</u>

It is assumed that the different spatial modes of a free-running laser will be incoherent to each other [36] and that there is no field interference; the photon density in any specific layer is determined by the sum of the photon density which every individual mode carries in this layer. Furthermore, since the power (or photon density) distributions of the modes are symmetric, the photon-carrier interaction is identical in both halves of the laser, and only half of the layers need to be considered independently.

The approach will be to consider the carrier density in any layer j (N$_j$) and the photon density in any mode i (Γ_i). In a given layer j, the local gain (G$_j$), which is proportional to the imaginary part of the local refractive index of that layer, is defined:

$$G_j = -2Im(n_j)c/n. \qquad (4)$$

42
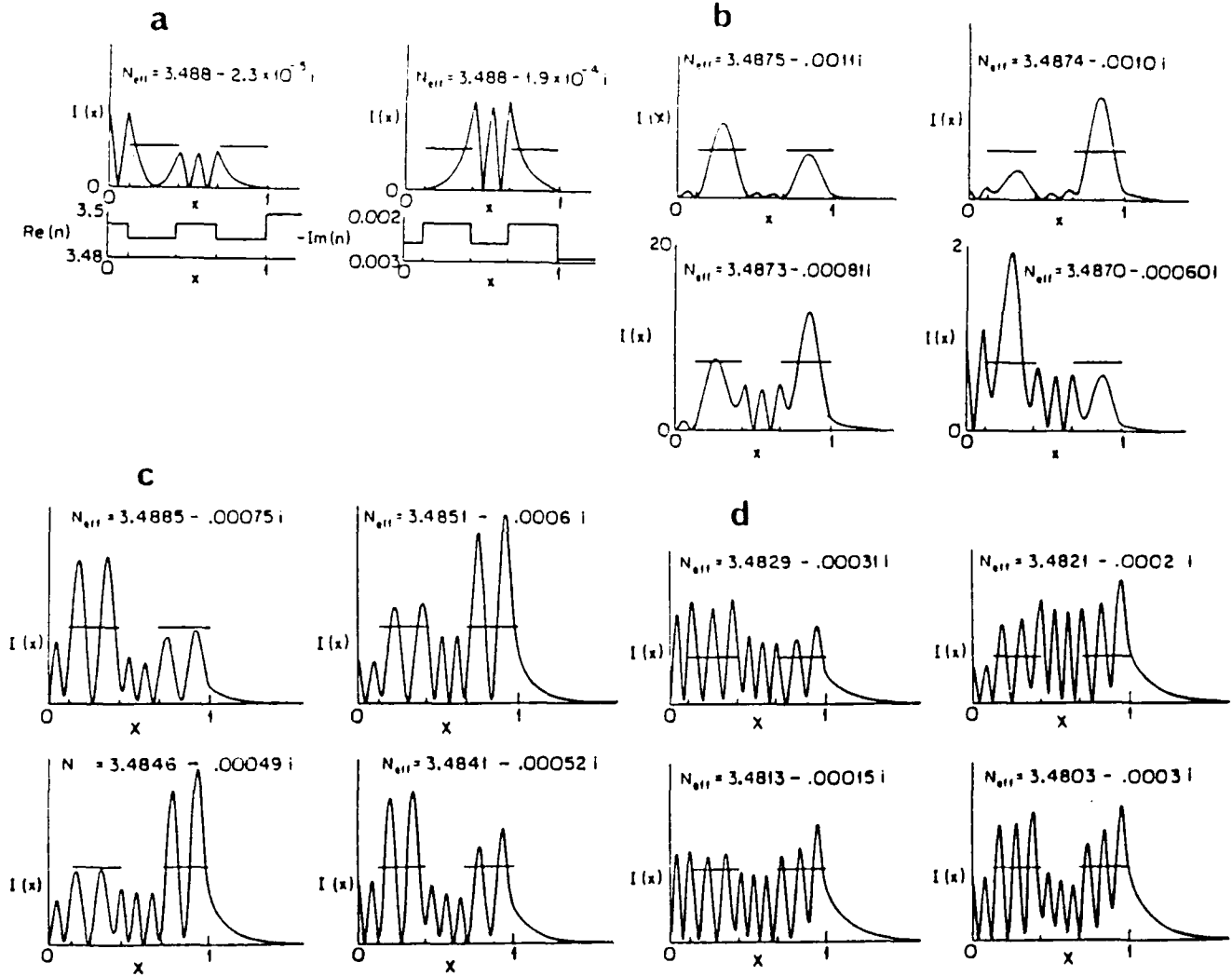
Figure 2. Intensity distributions, $I_i(x)$, for modes with positive gain within the step-index guide with complex refractive index shown in 2a. Because of symmetry only half the four-stripe geometry is shown. Fig. 2a also shows the only "index guided" modes. Fig. b,c,d shows the "gain-guided" modes, alternating even and odd modes. The horizontal lines on the intensity distributions mark the position of the high-current, high-gain stripes.

This relation transforms the gain per unit length into a gain per unit time by multiplying by the modal velocity. Since the refractive index varies only slightly, n is fixed as the value at transparency, when the imaginary part goes to zero.

Stimulated recombination in a particular layer j decreases the carrier density in that layer through a filling factor which calculates the fraction of the optical mode power which is in that layer:

$$\Gamma_{ij} = \int_{\text{layer } j} |E_i|^2 \, dx \; / \; \int_{-\infty}^{+\infty} |E_i|^2 \, dx \qquad (5)$$

The modal gain g_i is defined in terms of the imaginary part of the effective refractive index which is calculated for that mode through its effective refractive index n_{eff}:

$$g_i = -2\text{Im}(n_{eff})c/n. \qquad (6)$$

By considering only one single longitudinal mode but several transverse modes i, located within several layers j, the dynamic equations for laser operation can be written as [36].

$$\frac{dN_j}{dt} = \frac{J_j}{q\,d} - \frac{N_j}{\tau_s} - \sum_i \Gamma_{ij}\,G_j\,P_i \qquad (7.1)$$

$$\frac{dP_i}{dt} = \frac{c}{n}\,g_i\,P_i - \frac{P_i}{\tau_p} + \frac{\gamma}{\tau_s}\sum_j \Gamma_{ij}\,N_j \qquad (7.2)$$

The first equation represents the rate of increase of the carrier density in the j-th layer, which is a function of the injected carrier rate (q is the electron charge and d the active layer thickness), spontaneous recombination (controlled by τ_s), the spontaneous lifetime τ_s, and the stimulated recombination produced by all of the present modes. The decrease in carrier density in the jth layer due to stimulated emission is summed over all modes i with the fraction of intensity of each mode in layer j given by the overlap integral Γ_{ij}.

The photon lifetime within the cavity τ_p depends on the cavity length and the reflectivity of the front facets of the laser. Since the in-plane beam divergence is very small, all of the modes are going to experience very similar reflection, and τ_p can be assumed independent of the mode. Finally γ is the spontaneous emission factor and the filling factors have been included to allow the different layers to have a different contribution to the fraction of spontaneous emission coupled into the mode. This is not a crucial point since this term is negligible once the mode has been excited in the cavity.

44

Since the gain is proportional to the carrier density, equations (7) can be written in terms of two independent variables, one containing the photon densities of the modes, and the other either the carrier densities or the gains per time unit in the layers.

F. Method of Simulation

The simulation considers small time intervals such that the parameters vary a negligible amount along them. Then the right hand side of equations (7) can be considered constant in the interval, and the rate of variation of photons and carriers linearized. It is enough to use a simulation interval on the order of one tenth of the smallest time constant involved τ_p. In any step the carrier density is calculated in all of the layers. This carrier density determines the refractive index distribution by using equation (3). The propagation constants of the modes will then be obtained, and the filling factors calculated by (5) for all of the modes with a positive gain. For the step-index multilayer structure, these factors have analytical expressions, so that no numerical integration is necessary. All of these modes will be considered for the new calculations of the photon density in any mode, and the carrier density in any layer for the next step.

The calculation of the propagation constants of the modes is important, since the refractive index profile varies in any step. The eigenvalues must be found for all the important modes. This simulation includes the four modes with highest gain, which are the three first modes of figure 2b, and the first one of figure 2c. It will be found in the example calculated that only two of these modes are involved in mode competition, since the other two never reach threshold. To obtain the initial guesses for the first step of the simulation, an initial waveguide (i.e., a nonzero carrier density) must be defined, so that all of the modes can be identified and their propagations constants obtained.

In the initial moments of the turn-on event, the photon density of all of the modes can be considered zero, and then equation (7.1) has an analytical solution:

$$N_j = \frac{\tau_s}{q\,d} J_j \left[1 - \exp\left(-\frac{t}{\tau_s}\right)\right] \qquad (8)$$

Since the current is identical in all of the gain stripes as well as in all of the gaps during this situation, the array consists of identical waveguides. This situation will vary in the moment that the first mode reaches a positive gain, and P_1 is no longer zero. Solving a waveguide problem such as the one

45

defined in the previous section, keeping a fixed ratio r_J between the gaps and the gain elements, determines the threshold carrier density N_{th} at which the first mode has zero gain. This gives the propagation constants of the four modes used as the initial guesses of the first simulation step. This means that the simulation starts at a certain time after the bias current is switched on, given by

$$t_{th} = - r_s \ln[1 - \frac{q\ d\ N_{th}}{r_s\ J_g}] \qquad (9)$$

where J_g is the current density in the gain elements.

G. Numerical Results

The numerical model described above was applied to the simulation of turn-on transient events in a four-stripe array. Injection currents varied from 100 to 600 mA. The threshold current for laser operation was found to be at about 156 mA. Fig. IV-3 represents the transient behavior of the turn-on event for bias currents of 200, 300, 400 and 500 mA. In each case the upper curves represent the gain variation of the modes while the lower curves represent the average photon density of the modes within the cavity. The horizontal line represents the mirror losses. In steady state, gain equals loss so that the power remains invariant. In the first two cases, only the first mode is excited, while in the other ones we can see the mode competition problem. At a bias current of 400 mA, the first mode is first excited, while the gain of the second one does not reach the mirror losses. As its gain increases, the second mode starts oscillating so that a part of the output power goes to it. The total output keeps on oscillating around the same value, but the average photon density of the first mode decreases as the photons of the second mode induce the recombination of a part of the carriers. Finally both modes tend to a steady state in which both gains equal the radiation losses. At 500 mA the array solves the mode competition problem in a different way. Once the second mode appears, the gain of the first mode starts decreasing to a steady state below the radiation losses, so that this mode stops lasing, and its power goes to zero. Only the second (even) mode oscillates in this case. This situation (only second mode oscillating in the steady state) is maintained, at least up to 600 mA.

The reason for the mode coexistence or only one dominating mode can be seen by observing the normalized intensity distributions of the two involved modes, which are shown in Fig. IV-4. Both at 200 and 300 mA the first mode has a very regular intensity distribution, with aproximately equal lobes in the gain regions. At 400 mA, however, the situation is completely different. The intensity of mode one in the inside elements of
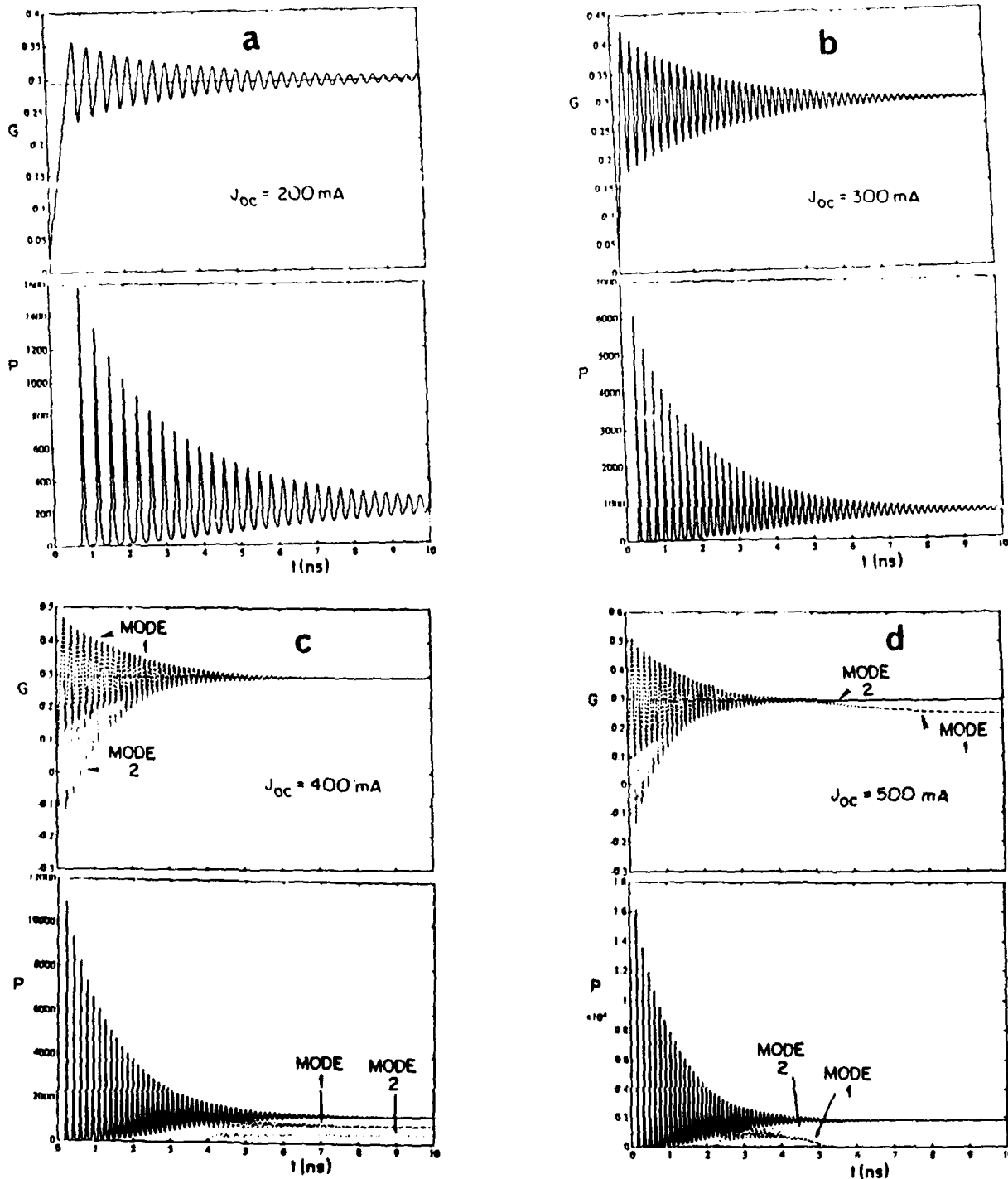
Figure 3. Modal gain (top figure in each group) per unit time, and average photon density per mode (bottom figure), as a function of time after turn-on of four-element gain-guided laser array when pumped by the DC current, J_{DC}, shown. In a) and b) only the highest-gain mode (mode 1) turns on. In c) the dashed curve represents mode 1 and the dotted curve represents mode 2. The total photon density is shown as the solid line. Mode 2 turns on after 4 ns and robs power from mode 1. As time evolves the gain of both modes eventually clamps at threshold. In d) the power in mode 2 turns on after 2 ns and robs power from mode 1, causing it to turn off after 5 ns when its gain decreases below threshold.
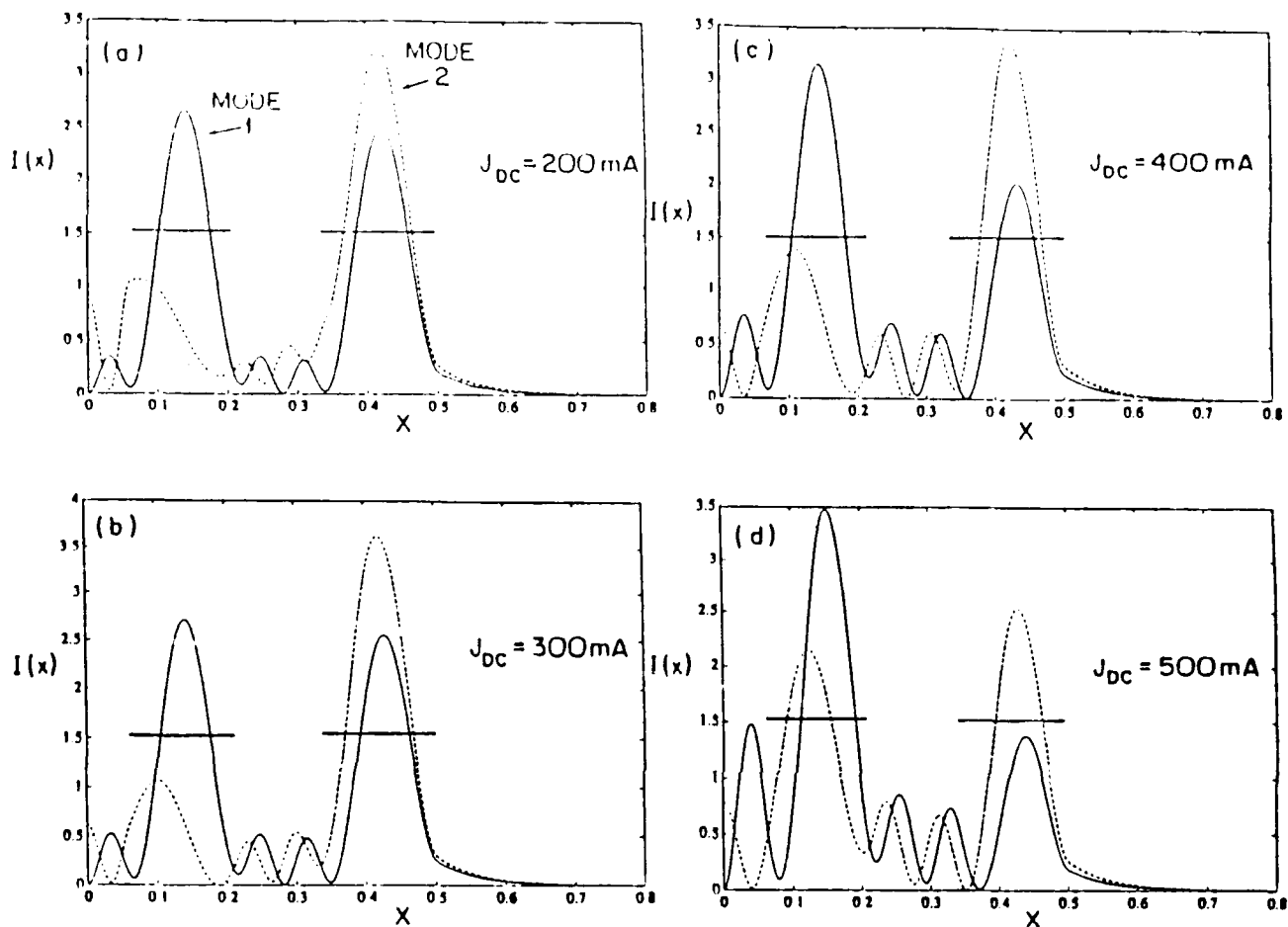
47

Figure 4. Near-field intensity profiles $I_i(x)$ for modes 1 and 2 at the DC current levels shown, J_{DC}, in the absence of stimulated emission. By comparing intensity profiles, mode competition can be understood. The distance scale is normalized to the guide full-width. Position of the high-gain stripes is marked with horizontal lines.

48

the array is higher than that of the outside ones, inducing the recombination of more carriers, hence a lower gain. This situation is ideal for the excitation of mode two, where the power distribution in the gain elements is opposite. So those modes are very comfortably excited without competing for the gain. At 500 mA, however, the increase in the gain changes the refractive index distribution so that mode two now presents approximately equal lobes, while mode one presents very uneven ones, interacting with carriers in a less efficient way. The final near and far field patterns in steady state are presented in figure 5, where at 200, 300 and 500 mA they coincide with those of the dominant modes, while at 400 mA the curves are given by the adequate weight of the two modes according their respective relative powers. It can be seen that now the total intensity distribution is very well balanced between the inside and the outside gain elements.

When mode competition problems arise, it is interesting to check if the steady state solution is really a stable point or if if it depends on the previous history of the laser. In order to check that we perturbed the situation after the first 10 nanoseconds, by adding an input current pulse of 50 mA and 5 ns over the bias. After a reasonable time, the same steady state was reached. This happened at all of the currents. Figure IV-6 shows the photon number evolution for the case of a 300 mA bias current as an example. This is the most interesting case because during the pulse the second mode is excited, and both of them co-exist while the current is kept at 350 mA, but the second mode rapidly disapears after the perturbation pulse is over.

H. **Results**

Numerically modelling of gain-guided four-stripe arrays explicates the effect of mode competition on the determination of steady-state operating conditions. The modes of the overall transverse waveguiding structure were used as the foundation for the calculation, neglecting interference between these modes. Instabilities in neither any one mode, nor in the total output were seen, in contrast to the coupled-mode approach [20], [21]. However, since the output appears as two modes, if only a portion of the output is observed, the modes are expected to interfere, resulting in oscillations at the frequency difference between the two modes. This beating will be seen in the noise spectrum of the output. Estimates of the expected frequency for such beating is shown here.

From the requirement that the field go to zero at the mirrors of a resonator,

$$n_{eff}kL = m\pi.$$

Using $k = 2\pi\nu/c$, any fractional change in refractive index will
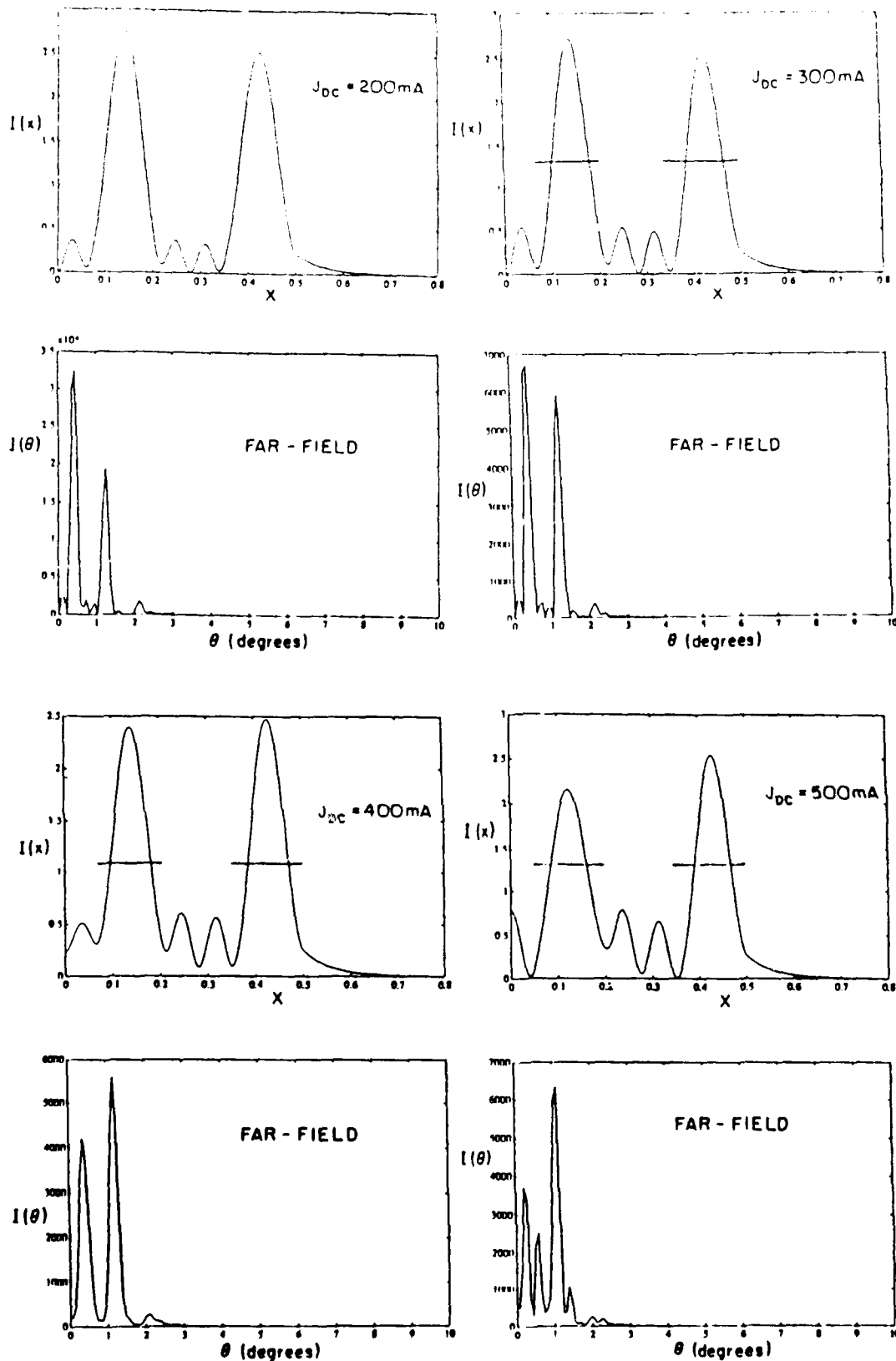
49

Figure 5. Near-field (upper curves) and far-field (lower) intensity distributions for the steady-state case of a four-stripe gain-guided array determined by the numerical simulation shown in Figure 3. In both cases only half of a symmetric distribution is shown. DC current level J_{DC} is indicated.

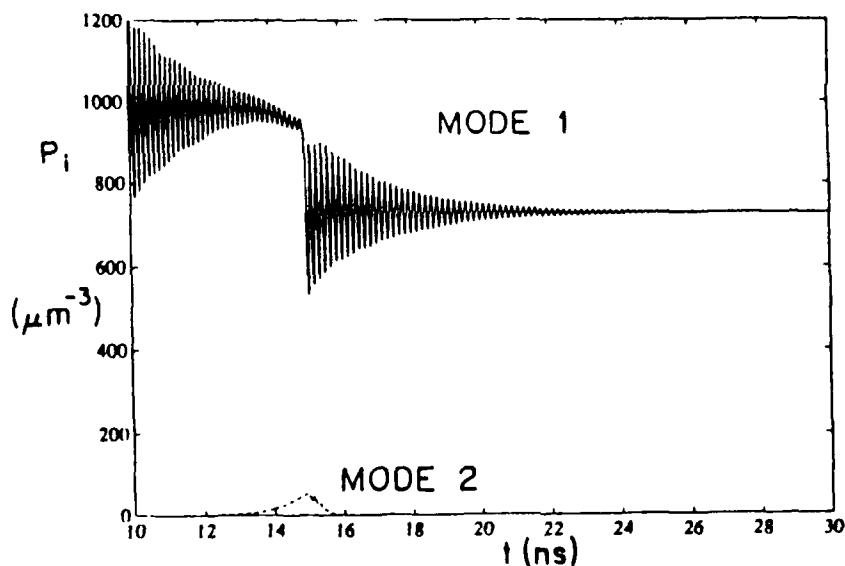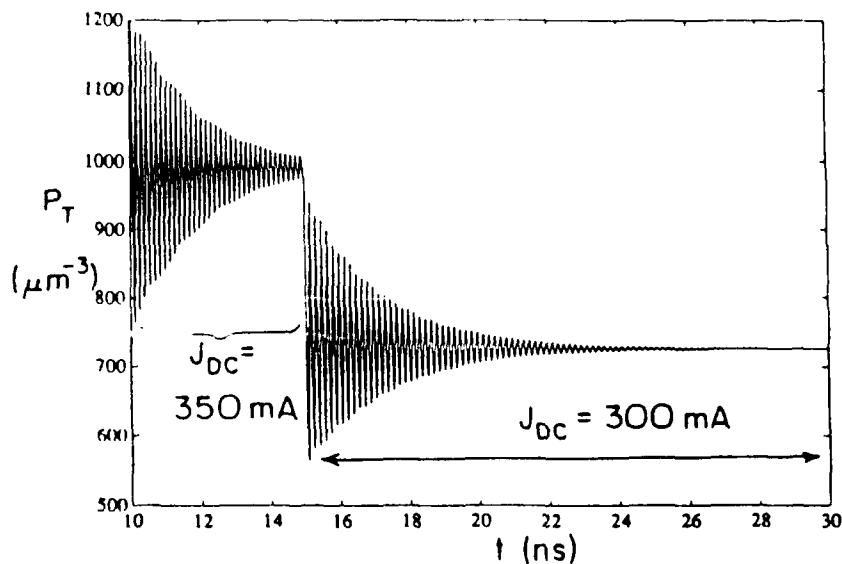**Figure 6.** Response of the laser, driven in steady-state at 300 mA to a perturbation of 50 mA. Figure begins at 10 nsec, after the laser has achieved steady-state, with an abrupt step of 50 mA. In the presence of 350 mA, power in mode 2 begins to grow. However, when the perturbation is removed, the power in mode 2 quickly decays and the steady-state of only power in mode 1 is again achieved.

51

lead to a change in frequency given by

$$\delta n_{eff}/n = \delta \nu / \nu \quad \text{or} \quad \delta \nu - (\delta n_{eff}/n)(c/\lambda).$$

From the data in Fig. IV-3, $dn_{eff}/n = 3 \times 10^{-5}$ and $\delta \nu - 10^{10}$ Hz, too fast for us to see in our experiments.

However, it is expected that the four-stripe lasers will have modes spaced farther away than the ten-stripe arrays. This means that interference between the modes in a ten-stripe array may occur at a lower frequency, one low enough to be seen in the noise measurements. An estimate of this effect can be made by assuming that the lowest modes scale similar to those in well-confined guides, for which

$$n_{eff} = \bar{n}_c[1 - (m\pi/2V)^2],$$

where V is the normalized guide-width. The two lowest-order modes have a separation given by

$$dn_{eff}/n = (3\pi/2V)^2.$$

Thus, for a ten-stripe guide, with V which is 2.5 times larger than a four-stripe guide, the modes are expected to be six times closer spaced in frequency, bringing them down close to the GHz region, where such instabilities can be measured. GHz instabilities have been seen experimentally with streak cameras by the group at Oregon Graduate School, and we believe that the analysis described here explains such phenomena. That is, it is interference between the several modes which may oscillate simultaneously in a gain-guided array.

There remains one serious approximation in this analysis, the neglect of interference between the modal fields. This should be done in a further study.

I. References to Section IV

[1]. Statz, H., and Tang, C.L., "Multimode oscillations in solid-state masers", J. Appl. Phys. 35, 1377-1383 (1964).

[2]. Hauck, R., Hollinger, F., Weber, H., "Chaotic and periodic emission of high power solid state lasers", Opt. Commun. 47, 141-145 (1983).

[3]. Wang, C.P., Varwig, R.L., "Competition of longitudinal and transverse modes in a CW HF chemical laser", Opt. Commun. 34, 103-107 (1980).

[4]. Biswas, D.J., Harrison, R.G., "Observation of pulsating instabilities and chaos in a transversely excited atmospheric pressure CO_2 laser", Opt. Commun. 57, 193-195 (1986).

[5]. Biswas, D.J., Dev, V., and Chatterjee, U.K., "Experimental observation of instabilities and chaos in the secondary-beat frequency of a multiple-transverse-mode CO_2 laser", Phys. Rev. A 38, 555-558 (1988).

[5]. Wang, S.S., Winful, H.G., "Dynamics of phase-locked semiconductor laser arrays", Appl. Phys. Lett. 52, 1774-1776 (1988).

[7]. Winful, H.G., Wang, S.S., "Stability of phase locking in coupled semiconductor laser arrays", Appl. Phys. Lett. 53, 1894-1896 (1988).

[8]. Elliot, R.A., De Freez, R.K., Paoli, T.L., Burnham, R.D., Streifer, W., "Dynamic characteristics of phase locked multiple quantum well injection lasers", IEEE J. Quantum Electron, QE-21, 598-602 (1985).

[9]. DeFreez, R.K., Bossert, D.J., Yu, N., Elliot, R.A., Winful, H.G., "Spectral and picosecond temporal properties of flared guide Y-coupled phase-locked laser arrays", Appl. Phys. Lett. 53, 2380-2382 (1988).

[10]. Botez, D., Peterson, G., "Modes of Phase-locked diode-laser arrays of closely spaced antiguides", Electron. Lett. 24, 1042-1043 (1988)

[11]. Lang, R.J., Yariv, A., "Analysis of the dynamic response of multielement semiconductor lasers", IEEE J. Quantum Electron. QE-21, 1683-1688 (1985).

[12]. Marshall, W.K., Katz, J., "Direct analysis of gain-guided phase-locked semiconductor laser arrays", IEEE J. Quantum Electron. QE-22, 827-832 (1986).

[13]. Buus, J., "Principles of semiconductor laser modelling", IEE Proc. vol. 132, Pt. J, 42-51 (1985).

[14]. Butler, J.K., Evans, G.A., Carlson, N.W., "Nonlinear characterization of modal gain and effective index saturation in channeled-substrate-planar double-heterojunction lasers", IEEE J. Quantum Electron. qe-25, 1646-1652 (1989).

[15]. Streifer, W., Kapon, E. "Application of the equivalent-index method to DH diode lasers", Appl. Opt. 18, 3724-3725 (1979).

[16]. Buus, J., "The effective index method and its application to semiconductor lasers" IEEE J. Quantum Electron. QE-18, 1083-1089 (1982).

[17]. Baets, R., Lagasse, P., "Longitudinal static-field model for DH lasers", Electron. Lett. 20, 41-42 (1984).

[18]. Twu, Y., Wang, S., Whinnery, J.R., Dienes, "Mode characteristics of phase-locked semiconductor laser arrays at and above threshold", IEEE J. Quantum Electron. QE-23, 788-794 (1987).

[19]. Hadley, G. R., Hohimer, J. P., Owyoung, A., "Comprehensive modelling of diode arrays and broad area devices with applications to lateral index tailoring", IEEE J. Quantum Electron. QE-24, 2138-2152 (1988).

[20]. Botez, D., Mawst, L.J., Peterson, G., "Resonant leaky-wave coupling in linear arrays of antiguides", Electron. Lett. 24, 1328-1330 (1988).

[21]. Botez, D. Mawst, L.J., Peterson, G., Roth, T.J., "Resonant optical transmission and coupling in phase-locked diode laser arrays of antiguides: The resonant optical waveguide array", Appl. Phys. Lett. 54, 2183-2185 (1989).

[22]. Yeh, P., Yariv, A., Hong, C.-S., "Electromagnetic propagation in periodic stratified media. I. General theory", J. Opt. Soc. Am. 67, 423-438 (1977).

[23]. Ghatak, A.K., Thyagarajan, K., Shenoy, M.R., IEEE J. Lightwave Technol. LT-5, 660-664 (1987).

[24]. Coldren, L.A., Koch, T.L., "Analysis and design of coupled-cavity lasers - Part II: Transient analysis", IEEE J. Quantum Electron. QE-20, 671-682 (1984).

V. CONCLUSIONS

1. COMPARISON OF ARRAY WITH SINGLE LASER IN SYSTEMS APPLICATIONS

Experimental results show that single-mode single-element lasers have better noise performance than the arrays measured here (about 15 to 20 dB better in the RIN). But arrays give much more power than single lasers. This section makes a comparative study on the performance of an array versus a single-element laser for system uses, considering their noise performance and the power output simultaneously.

Following a similar calculation as given in section II.4., SNR_{th}, SNR_{shot} and SNR_{RIN} are calculated for a given power level for both the array and a single laser. For calculating SNR_{RIN} it has been assumed that, for array, RIN = -135 dB/Hz (typical, measured) and for a single laser, RIN = -150 dB/Hz (typical, ref. 1). A modulation index of 4% is assumed along with a band-width

54

of 4 MHz as in section II.4. The total signal to noise ratio SNR_{tot} is calculated using,

$$1/SNR_{tot} = 1/SNR_{th} + 1/SNR_{shot} + 1/SNR_{RIN} \qquad (23)$$

and plotted as a function of the detected optical power (Fig. V-1). As can be seen, the system SNR saturates at high optical power (for $P_0 > 1$ mW), due to the laser RIN. In this regime, using an array instead of a single laser will not be advantageous as far as the system SNR is concerned. However, since an array can deliver much more power than a single element laser, the array will give better SNR performance for lower detected powers. For example,

SNR for single laser (for $P_0 = 0.01$ mW) = 30 dB

SNR for array (for $P_0 = 0.1$ mW) = 37 dB

Thus if the detected power level is less than 0.01 mW for a single laser of RIN = -150 dB/Hz, then the system SNR would improve if the laser is replaced by an array (with RIN = -135 dB/Hz) which will give 10 times more optical power. In the present example an improvement of up to a maximum of 20 dB in the system SNR is possible for sufficiently weak inputs.

For some practical situations one may require better SNR than 38 dB (which is the upper limit in this example). We have shown that this is possible by increasing the modulation index, resulting in SNR as high as 48 dB.

Conclusions

    a.   There is no advantage of using an array (as far as the system SNR is concerned) if the received optical power is sufficiently high.

    b.   System SNR can be improved up to 20 dB, if an array is used instead of a single laser (assuming an array delivers 10 times more power than a single laser) for low detected powers.

    c.   Low-frequency modulation may be used to reduce the RIN. At higher bias current, with modulation at 10 MHz, it is possible to reduce the RIN by 10 dB to -145 dB, increasing the SNR by 10 dB. Thus, the best possible SNR with the arrays measured here is 48 dB, achievable with both gain-guided and index-guided arrays, using 10 MHz modulation.

2. MODE-COMPETITION IN LASER ARRAYS

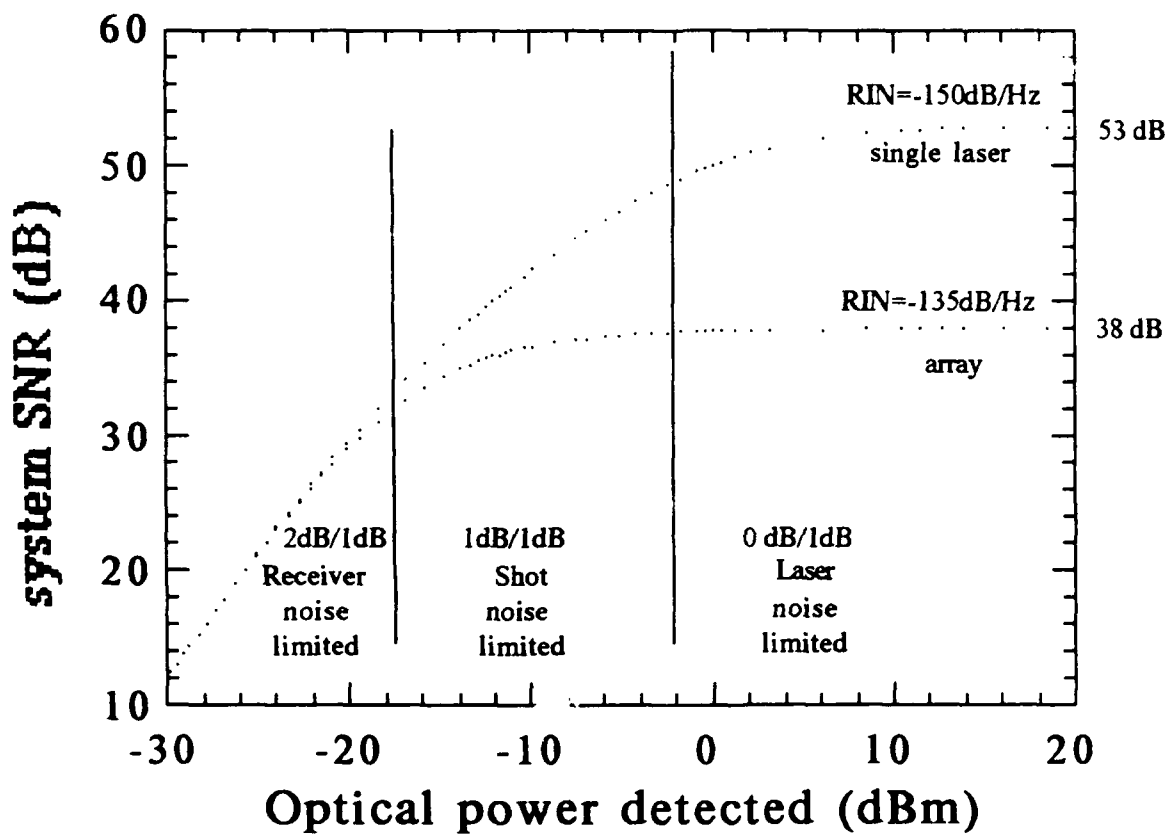As a result of the modelling it is seen that the laser array

Fig.V. The system SNR as a function of received optical power for a single mode laser and an array. A modulation index of 4% and a band-width of 4 MHz were assumed for the calculation.

usually operates in several transverse modes. Competition between these modes leads to excess noise over that measured in single-element diodes. It is believed that modulation under the appropriate conditions can reduce this competition, yielding results which are closer to single-element devices. It is already known that gain-guided single-element lasers can have excess noise over index-guided lasers, due to transverse mode-competition. It is already known that DFB lasers have the lowest noise of all, due to the absense of both longitudinal and transvserse mode competition.

The result of this study is that the lowest noise in a laser array will be possible only if both the transverse and longitudinal modes are limited. This can be done by placing the array in a transvserve-mode-selecting external cavity along with a grating, to reduce longitudinal modes. The noise in such a cavity should be comparable to that measured with DFB lasers.

3. SUGGESTIONS FOR FUTURE WORK

a. Quantitative measurement of mode competition noise

As we have observed in the present study, the arrays are noisier than single-mode lasers. The theoretical analysis indicates that the increased RIN in laser arrays come from mode competition between the two lowest order modes which choose to oscillate in an array. The measurement was performed at the farfield collecting only a portion of the output light emitted from the array. The extra noise arising from mode competition can be estimated by comparing the noise in the total output light (collecting all the output light) to the noise in a portion of the output light. In addition, the possible mode partition noise exhibited by the longitudinal modes in the array may be decomposed from the mode competition noise between the transverse modes by using the fact that the longitudinal modes are separable in the frequency domain. Thus, measuring the noise at a given frequency, with a given spatial extent, will allow a separation of the different effects. Such a study is important for further understanding of the various noise processes and ways to eliminate mode competition noise in an array.

b. Reduction of Noise in Mode-Selecting Cavity

Transverse and longitudinal mode selection are possible by using an external cavity. Although this is not usually wanted in optical communication systems, where sources should be small and cheap, for applications such as frequency standards a compact mini-cavity which includes both transverse and longitudinal mode selection may have a noise floor approaching that of the DFB laser, -160 dB. Such a cavity should be built and its noise properties measured. Longitudinal mode-selection could be by using a grating. Transverse mode-selection could be by using

hole-coupled optics, as demonstrated by Chang-Hasnain.

After noise-reduction in an external cavity is demonstrated, it may be possible to build a compact integrated optics or fiber optics version of the low-noise array source.

c. Study of noise in the presence of optical feed-back

The stability of the lasing modes is an important factor in determining the noise performance of a laser. Especially in arrays, where phase locking stability is a major concern, the investigation of the stability of output power in the presence of small external reflections (such as arising from a grin focussing lens or fiber facet) would be of considerable interest. Since any instability in the output power would appear as intensity noise, measurement of RIN as a function of optical feedback for low-noise arrays could be an important direction for further research to improve mode stability. No research on such stability has been published when noise is reduced by modulation.

4. REFERENCES TO SECTION V

V-1. Ken-ichi Sato, "Intensity noise of semiconductor laser diodes in fiber optic analog video transmission" IEEE J. Quantum Electron., vol. QE-19, pp.1380-1391, September 1983.

MISSION

of

Rome Air Development Center

RADC plans and executes research, development, test and selected acquisition programs in support of Command, Control, Communications and Intelligence (C³I) activities. Technical and engineering support within areas of competence is provided to ESD Program Offices (POs) and other ESD elements to perform effective acquisition of C³I systems. The areas of technical competence include communications, command and control, battle management information processing, surveillance sensors, intelligence data collection and handling, solid state sciences, electromagnetics, and propagation, and electronic reliability/maintainability and compatibility.